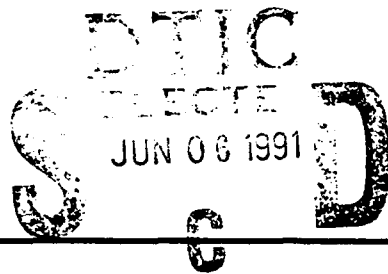


SRI International



Approved for public release
distribution unlimited

Final Report • May 1991

ULTRAFAST LASER TECHNIQUES

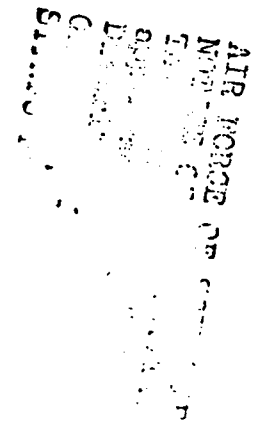
H. Helm, C. H. Becker, H. Bissantz, C. Bordas, M. J. Dyer, R. A. Copeland,
D. L. Huestis, and R. Kachru
Molecular Physics Laboratory

Contract No. : F49620-88-K-0006
SRI Project No. PYU-5541
MP 91-092

Prepared for:

Air Force Office of Scientific Research
Bolling Air Force Base
Washington, DC 20332

Attention: Dr. R. Kelley
Program Manager
General Physics Division
Directorate of Physics



and 19
12

91-01367



AD-A236 688



REPORT DOCUMENTATION PAGE			Form Approved OMB No. 0704-0188	
Public reporting burden for this collection of information is estimated to average 1 hour per response, including the time for reviewing instructions, searching existing data sources, gathering and maintaining the data needed, and completing and reviewing the collection of information. Send comments regarding this burden estimate or any other aspect of this collection of information, including suggestions for reducing this burden, to Washington Headquarters Services, Directorate for Information Operations and Reports, 1215 Jefferson Davis Highway, Suite 1204, Arlington, VA 22202-4302, and to the Office of Management and Budget, Paperwork Reduction Project (0704-0188), Washington, DC 20503				
1. AGENCY USE ONLY (Leave blank)	2. REPORT DATE 910506	3. REPORT TYPE AND DATES COVERED Final 15 FEB 88-147 EB 91		
4. TITLE AND SUBTITLE Ultrafast Laser Techniques			5. FUNDING NUMBERS	
6. AUTHOR(S) H. Helm, C. H. Becker, H. Bissantz, C. Bordas, M. J. Dyer, R. A. Copeland, D. L. Huestis, and R. Kachru				
7. PERFORMING ORGANIZATION NAME(S) AND ADDRESS(ES) SRI International 333 Ravenswood Avenue Menlo Park, CA 94025			8. PERFORMING ORGANIZATION REPORT NUMBER MP 91-092 PYU-5541	
9. SPONSORING/MONITORING AGENCY NAME(S) AND ADDRESS(ES) Air Force Office of Scientific Research Bolling Air Force Base Washington, DC 20332			10. SPONSORING/MONITORING AGENCY REPORT NUMBER F49620-88-K-0006	
11. SUPPLEMENTARY NOTES DP				
12a. DISTRIBUTION/AVAILABILITY STATEMENT Approved for public release, distribution is unlimited			12b. DISTRIBUTION CODE	
13. ABSTRACT (Maximum 200 words) A subpicosecond wavelength-tunable high-power dye-laser has been developed and used to perform novel experiments on multiphoton ionization and dissociation, allowing us to draw important conclusions about modifications of the excited state structure of atoms and molecules when exposed to intense radiation. The laser system is based on a synchronously-pumped oscillator, a pulse chirping and compression device, and four amplifiers. The near-Gaussian spatial beam profile and high peak power (>10 GW) allow generation of extreme intensities (>10 ¹⁵ W/cm ²) lasting a few hundred femtoseconds, that when combined with wavelength tunability (580-670 nm and 300-330 nm) reach experimental regimes that were previously inaccessible. In molecular hydrogen we have shown for the first time that the intense field affects both the Rydberg and the core electrons prior to ionization. In atomic xenon we found that, over a limited range, the AC Stark shifts of the 4f, 5f, 6s, and 6d levels correspond to the ponderomotive shift of free electrons. We have also performed measurements of the magnitude and temporal dependence of the third-order nonlinear susceptibility of polymers. In another first we employed our laser to photoionize neutral atoms argon-ion-sputtered from various surfaces. The near-unit ionization efficiency provides an almost stoichiometric measurement of the surface composition.				
14. SUBJECT TERMS Multiphoton ionization, Stark, ponderomotive, intense fields, compression, axicon, femtosecond, Rydberg, core, free electrons, hydrogen, degenerate four-wave mixing (DFWM), polymers, surface analysis by laser ionization			15. NUMBER OF PAGES 68-includ. Appendices	
			16. PRICE CODE	
17. SECURITY CLASSIFICATION OF REPORT Unclassified	18. SECURITY CLASSIFICATION OF THIS PAGE Unclassified	19. SECURITY CLASSIFICATION OF ABSTRACT Unclassified	20. LIMITATION OF ABSTRACT UL	

INTRODUCTION

Many physical processes such as atomic and electronic motion in isolated molecules, intermolecular energy transfer and nuclear rearrangement, gas-phase-surface equilibration, and the dynamic response of lattices proceed in the picosecond and sub-picosecond time domain. As laser pulses have become shorter and shorter in recent years, it has become possible to initiate and to observe faster and faster phenomena. Thus each improvement in short pulse laser technology initiates new fundamental measurements and opens new phenomena to closer inspection.

The very notable achievements in sub-picosecond laser technology in recent years have thus allowed novel classes of experiments and the posing of questions into a time domain hitherto owned exclusively by theorists. While advancement has been substantial, strict experimental limitations still exist in techniques employed in this time domain because photon sources are frequently limited to a narrow range of wavelengths over which short optical pulses are produced.

The goal of our research work was to extend the commonly available wavelength range for intense ultrashort pulse lasers and to develop techniques for recording, processing, and measuring the spatial and temporal shape of ultrashort light pulses. This effort was intended to allow us to carry out novel experiments on isolated molecules subjected to very short laser pulses, photoelectron and photofragment spectroscopy in very intense laser fields, and phase conjugation in the sub-picosecond time domain.

The research described below was carried out using the SRI short pulse laser facility. The results obtained have expanded our fundamental understanding of the interaction of ultrashort laser pulses with matter and provided key knowledge, particularly in the field of interaction of intense short pulse radiation with atoms and molecules, as well as the application of such laser light as a diagnostic of the nonlinear response of matter and for surface diagnostics.

SUMMARY OF ACHIEVEMENTS

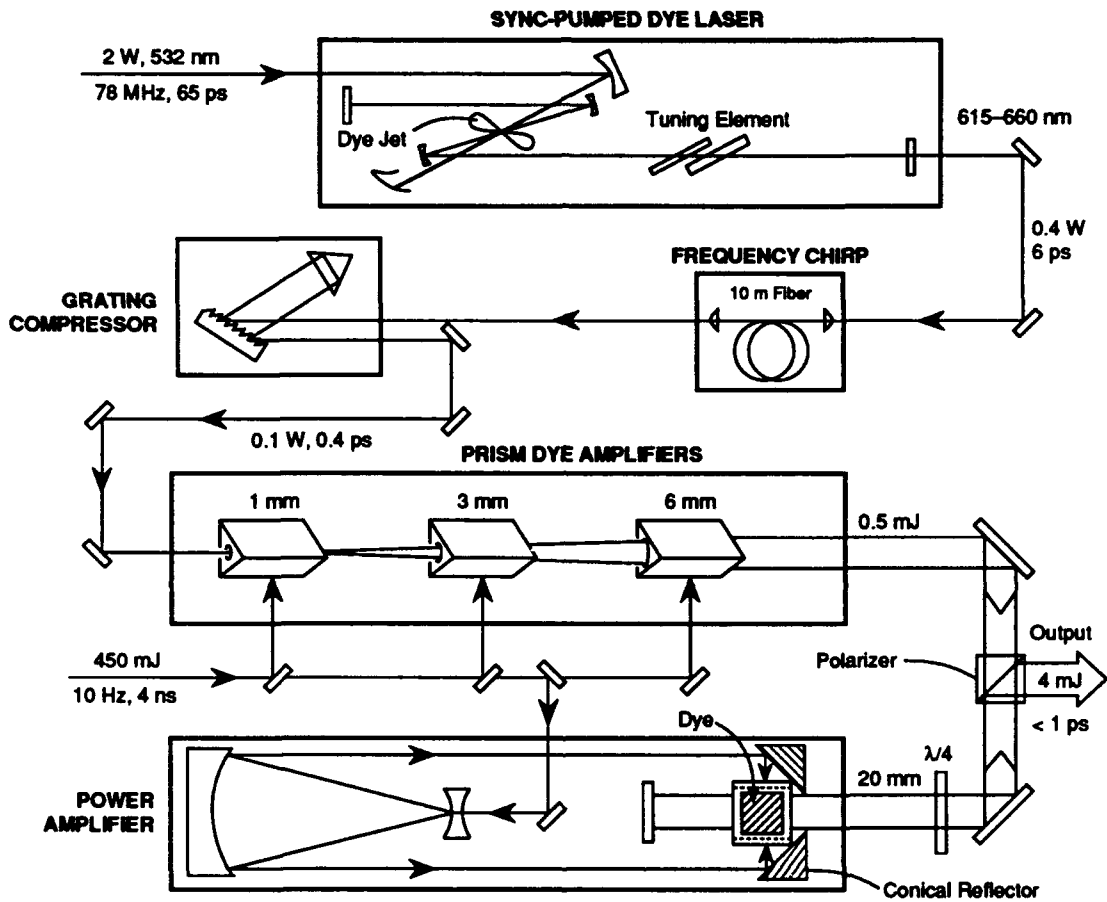
Our initial task in this project was to expand our experimental laser facility, including the design and development of a tunable, amplified dye laser system that delivers the most intense tunable light currently available. This sub-picosecond source reliably delivers focal intensities reaching 1×10^{15} W/cm².

In the course of this project, the resulting laser system was used in a variety of novel experiments, such as multiphoton dissociation and multiphoton ionization, studies of the competition between the two processes, four-wave mixing experiments, and surface analysis. These topics are discussed in detail below and in the appendices. Parts of the work have been presented at six conferences so far, and the principal investigator has been asked to give four invited lectures on these topics at international conferences this year.

Below we describe the specific achievements on the laser development and in the application of very intense laser pulses in novel experiments carried out under this project.

PRISM DYE AMPLIFIERS

A first effort was devoted to setting up an amplifier system for the output of a short pulse dye laser. For amplification up to pulse energies of approximately 500 μ J/pulse we chose three stages of prism amplifier cells, with diameters of 1 mm, 3 mm, and 6 mm, respectively. Our cell design is similar to that described originally by Bethune¹ for amplifiers pumped by an excimer laser. We have adapted this scheme to the beam profile of a Q-switched YAG laser by using cylindrical lens telescopes to match the pump beam geometry to the geometry of the prism cells. The cells are mounted on individual positioning stages that allow easy alignment, and spatial filters are placed between each stage to minimize the amplified spontaneous emission (ASE). With the three stages of amplification we routinely achieve amplification factors of 5×10^5 , which allows us to boost ten pulses per second of the output of the home-built modelocked dye laser from the nJ range into the 0.5 mJ range. A schematic diagram of the laser setup with amplifiers is given in Figure 1.



RM-8231-10

Figure 1. Layout of the tunable high power sub-picosecond laser system.

A dye laser is synchronously pumped by a commercial modelocked frequency doubled YAG laser. The dye laser is tunable from 5700 to 6700Å using the dyes R6G and DCM. The dye laser output is chirped and compressed first and then amplified in four successive dye amplifier stages.

AXICON AMPLIFIERS

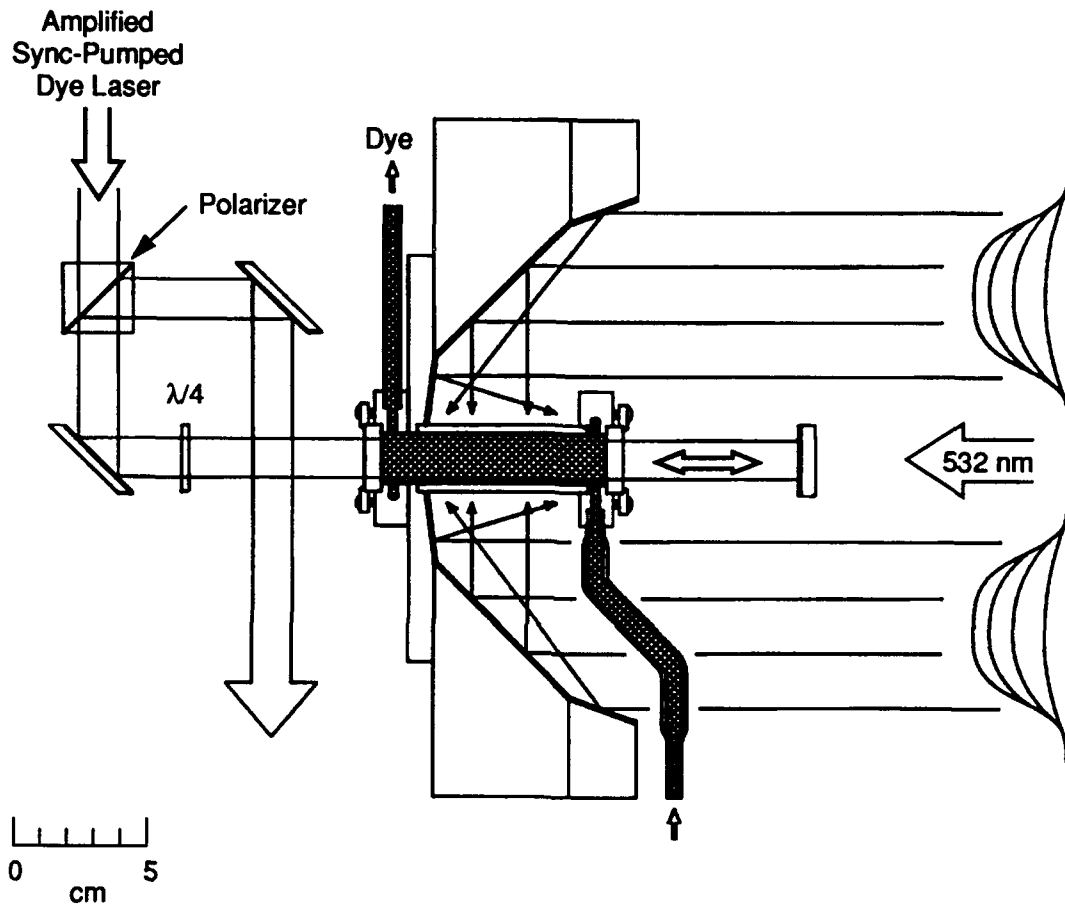
A fourth amplification stage has been added to the system in the form of a reflective axicon amplifier of a novel design. The amplifier medium is currently a liquid dye. A schematic diagram is given in Figure 2.

Our aluminum axicon amplifier forms a cost-effective final power stage capable of generating 2 mJ in pulse energies single-pass mode and over 4 mJ in a retroreflecting, double-pass geometry when pumped by 220 mJ from a frequency-doubled Nd:YAG laser. Peak intensities greater than 10^{15} W/cm² are reached in the amplified dye beam, with focusing geometries having f-numbers ≤ 20 .

Because nonlinear effects can produce phase-front distortions in the final stage of high-gain-saturated amplification, it is desirable that the beam introduced into the final amplifier be as large as possible. Axicon amplifiers easily permit this large beam amplification while avoiding beam distorting effects. In addition, the conical geometry of the axicon is particularly well-suited to pumping by doughnut-mode lasers and can be easily scaled-up in size for higher power applications.

Our axicon reflector is machined from a 10-inch diameter, 2-inch-thick disk of type 7076-T6 aluminum. Dimensions of the reflector are tailored to a doughnut-shaped beam profile with a 7.5-cm inner diameter and a 17.5-cm outer diameter at $1/e^2$ intensities. The reflector's surface is polished to produce an average reflectivity of 85%. Mounted at the center of the axicon is a flowing dye cell 2.5 cm in diameter and 6 cm long.

The output of the synchronously pumped dye laser operating on DCM dye is amplified to 500 μ J by the prism cell triple-stage amplifier chain and is expanded to 1.75 cm ($1/e^2$) diameter before being delivered into the axicon. Two amplifier configurations are used. With both geometries, the pump laser is expanded, collimated, and reflected into the axicon by a 75-cm-radius mirror. In single-pass mode, the dye beam is directed through the back of the amplifier and picked off by a 45° reflector. A double-pass amplifier geometry is accomplished by retroreflecting the beam immediately back through the axicon and using a polarizer/quarter-waveplate combination, in addition to about 2 meters of time-path length, to isolate the triple-pass amplifier from the backward-travelling light and couple out the amplified beam. Pulse energies exceeding 4 mJ in < 2 picoseconds over a wavelength range from 610 to 660 nm are readily attained in this geometry. Frequency doubling in KDP yields conversion efficiencies averaging 25% and energies > 1 mJ/pulse. A publication² describing this amplifier is included as Appendix A.



RM-5541-7

Figure 2. Axicon design and optical layout for double-pass amplification.
The clear diameter of this stage is 22 mm.

PULSE COMPRESSION

Several modes of pulse compression have been experimented with. From these experiments, two permanent setups have emerged, one for compression of the modelocked pulse train from the Nd-YAG laser and a second for compression of the tunable dye laser.

After the output of the modelocked Nd-YAG laser is frequency-doubled, approximately 8 W of infrared (IR) radiation is left over. This left-over radiation is either dumped into a water-cooled beam stop or directed into a pulse compression system that uses it to produce short IR pulses with a high repetition rate (78 MHz). The system is configured according to literature descriptions of pulse compressors³ but is unique in its compact layout.

Figure 3 gives the details of this infrared pulse compressor. The 90-ps, 1064-nm pulses from the Antares laser enter at the top left. This beam is expanded using a 2:1 telescope. Using a combination of a half-wave plate and a polarizer permits injection of a variable amount of IR power into a 40-m fused silica fiber by using a microscope objective. The length of the single-mode fiber was chosen for optimal chirping of the 1-3 W of IR radiation that we typically launch into the fiber. Self-phase modulation in the fiber expands the frequency spectrum of the light, and the associated positive group velocity dispersion sweeps the color content of the pulse in such a way that the red portion is on the leading edge and the blue portion on the trailing edge of the pulse. The red-to-blue chirp of the light that exits the fiber is compensated by a grating pair geometrically laid out so that the associated negative group velocity dispersion of the diffracted beams just compensates the chirp, thereby resulting in a temporally compressed pulse. In our home-built pulse compressor, the chirped beam exciting the fiber is first reconstructed with polarization in the plane of Figure 3 by using a quarter-wave plate. This beam is reflected onto a first grating in near-Littrow configuration. The angular dispersion introduced by the grating on the beam is not drawn in Figure 3, but a single ray leaving the grating at 65° is shown. This beam reaches an identical grating after reflection on three mirror surfaces. The three mirrors are merely introduced to fold the required dispersion length (75 cm) between the two gratings to fit in as small as possible a lab space. After travelling this distance, the dispersed beam fills the 2-inch grating length and is reflected back onto itself. This arrangement has the effect of a second grating pair; it doubles the compression factor and compensates for the spectral walk-off. A small tilt in the second grating permits the incoming and returning beams, before they reach the quarter-wave plate, to separate spatially just enough so that the compressed beam can be picked off with a 45° mirror and directed out of the compressor.

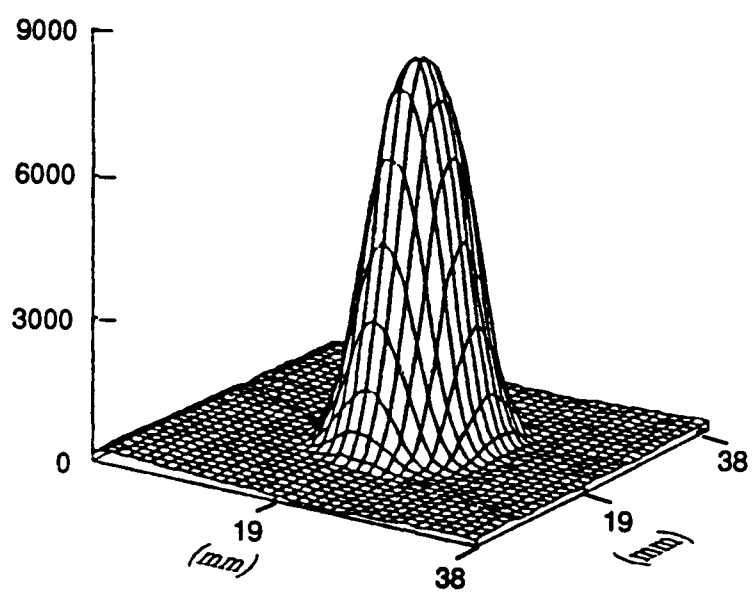
In our experiments, we can compress 90-ps IR pulses so that frequency doubling of the compressed output produces light with pulse lengths of ~ 5 ps. This light allows us to pump a second synchronously pumped dye laser system.

In addition, we have worked on amplification of chirped pulses from the dye laser (see Figure 1). We first send the dye laser output through a short piece of optical fiber to broaden the frequency spectrum and spread the pulse to ~ 60 ps duration, and subsequently compress the chirped pulse to typical pulse lengths of 300 fs. The average output power from the compressor is on the order of 30-50 mW and is fed through an optical diode into the four-stage amplifier chain. We have observed that a slightly chirped pulse needs to be injected into the amplifier chain to achieve the shortest output pulses from the amplifier. This observation shows that the dispersion of the pulse in the amplifier chain can be compensated for by injecting a slightly chirped pulse. This mode of operation has now been permanently adopted to achieve amplified pulses in the range of several milli/Joules at final pulse lengths below 1 ps. Figure 4 shows beam profiles of the dye laser before amplification and after pulse compression and amplification.

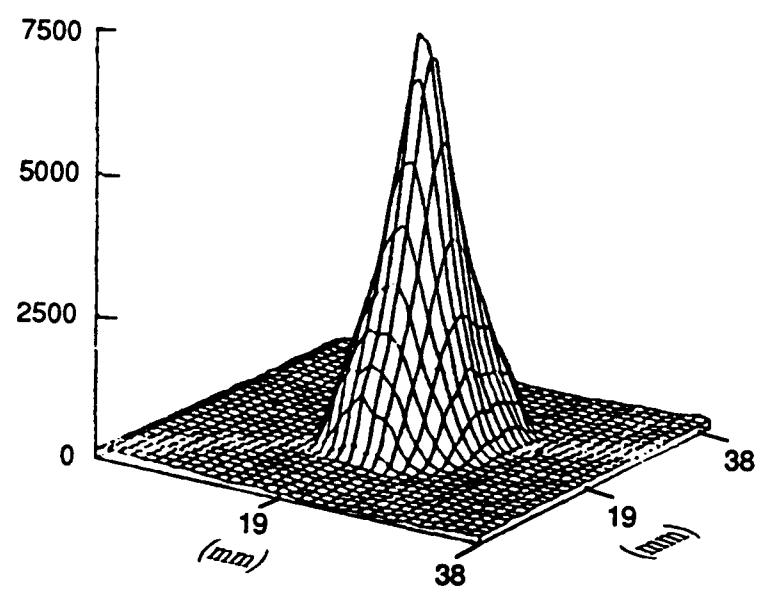
MULTIPHOTON IONIZATION

To demonstrate the high peak intensity that can be achieved with our short pulse laser, we have performed multiphoton ionization experiments; details of these experiments are reported in Appendix B.

Very intense laser fields drastically alter the energy level structure of atoms. Such modification occurs when the force exerted on the electron by the electromagnetic field of the laser becomes comparable to the atomic forces that bind the electron. As a consequence, multiphoton ionization in very intense laser fields is fundamentally different from low intensity multiphoton processes. A laser that is initially nonresonant with energy levels of the unperturbed atoms can become resonant as the intensity of the laser field grows, because the energy level structure of atoms can be drastically modified by the external electromagnetic field.⁵ A series of experiments on this subject have been performed over the past few years⁵⁻⁷ and nearly all of the experiments have used fixed-frequency lasers. At high frequencies of laser light, and over a limited range of photon energies, current theory predicts a one-to-one relationship between the detuning from the zero-field resonance and the field intensity required for the ac Stark shift to become resonant. We have begun to test this basic relationship in a systematic study of the ac Stark shift in xenon as a function of wavelength. To check our apparatus and laser setup, we first repeated Freeman's fundamental experiment on the ac Stark shifted resonance peaks in xenon at 6200 Å. Our photoelectron energy spectrum is shown in Figure 5. It was obtained using pulses of 40 μ J at about



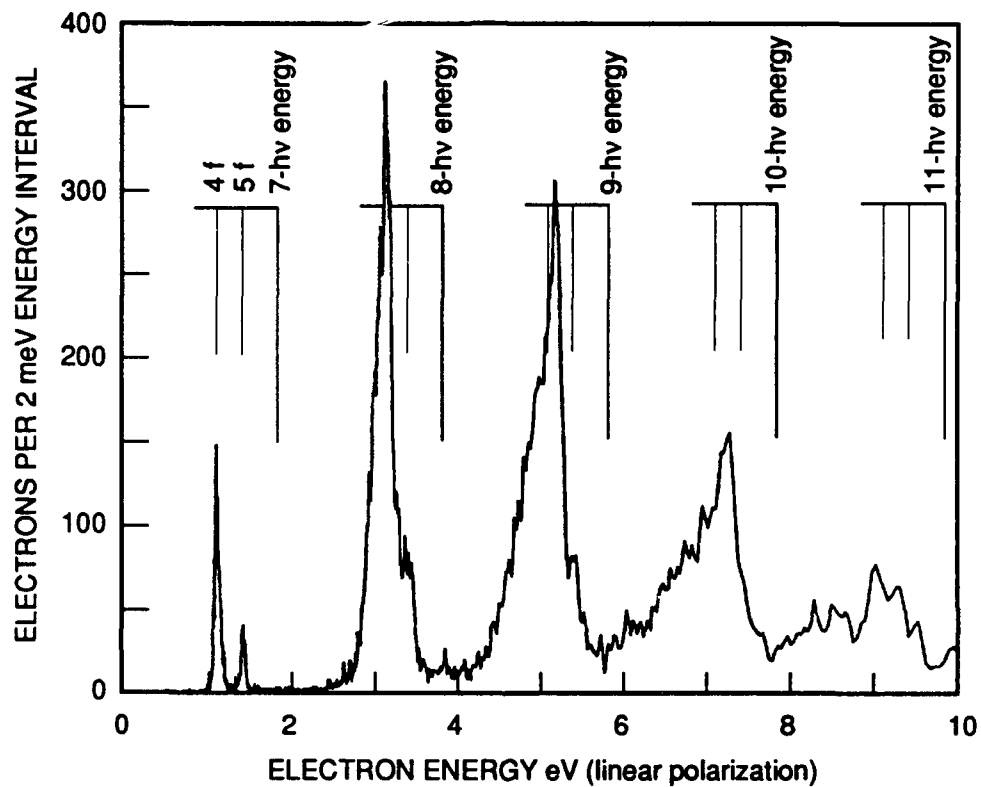
(a) After pulse compression



(b) After full amplification

RA-5541-010

Figure 4. Measured laser beam profile.



RM-5541-9

Figure 5. Photoelectron energy spectrum from 7-photon ionization of Xe at $200 \mu\text{J}$ at 6200\AA , $\sim 2 \text{ ps}$.

This spectrum shows that ac Stark shifting of excited xenon leads to resonant 6+1 photo ionization. Above-threshold ionization features carry the signature of multi-photon absorption by the electron before it leaves the atom.

1.5 ps. Nonresonant 7-photon photoionization at this wavelength should produce photoelectrons at 1.8 eV for the production of $\text{Xe}^+(^2\text{P}_{3/2})$. What is observed, however, are peaks that are shifted to lower energies, corresponding to resonant ionization via the shifted 4f and 5f levels. These shifts indicate that focal intensities exceed $1.5 \times 10^{13} \text{ W/cm}^2$ for this laser condition. Since the laser was attenuated to 1% of its average pulse energy, we conclude that at full illumination the peak intensity exceeds 10^{15} W/cm^2 . The discrete energy structures disappear if the full laser intensity is applied.

We then used the narrow UV light generated by the amplifier described above to study wavelength dependence of resonant multiphoton ionization of xenon. In the wavelength range from 305 to 330 nm, we recorded photoelectron spectra at pulsewidths of 1-2 ps at intensities reaching 10^{14} W/cm^2 . We observed sharp peaks in the photoelectron spectra that shift approximately linearly with the applied photon energy. These peak shifts indicate ionization paths that become resonant through the ac Stark shift, and for a number of peaks we have identified the contributing energy levels of xenon. Appendix B describes this work.⁴

TIME-DELAYED TWO-PHOTON IONIZATION

As a first step to test the feasibility of wavepacket experiments using single, isolated atoms or molecules, we transported the short pulse laser beam over a distance of 35 m to the fast neutral beam spectrometer, which is situated in a nearby laboratory. At that point the laser beam, which had expanded to about 2 cm in diameter, was recollimated using a telescope and split into two beams, one of which could be time-delayed up to 1 ns with respect to the other. The laser was tuned into resonance with the 3d-2p transition in triatomic hydrogen (5978 \AA). The time-delayed portion of the beam was used to photoionize the 3d state, and the resulting H_3^+ ions were detected. At modest beam intensities, the picosecond laser was able to saturate both the excitation and the ionization steps by using a single molecule per laser shot.⁸ We were able to delay the ionization step by up to 1 ns and still fully recover the ionization signal. This achievement indicates that experiments on an electron wavepacket formed in states with high principal quantum number by using a single atom are quite feasible, and promises the ability to demonstrate the predicted revival of electron wavepackets.⁹⁻¹⁰

OPTICAL PHASE CONJUGATION

Degenerate four-wave mixing (DFWM) is a nonlinear optical technique that is widely used as a spectroscopic tool and as a method of producing optical phase conjugation.⁴ This technique has potential application to data and image processing and, when used with short light pulses, is also a useful diagnostic tool for measuring the response and decay time of nonlinear optical

materials. We have set up a computer controlled experiment for measuring absolute phase-conjugate reflectivities and for determining the temporal response of materials in the picosecond regime. The general layout is shown in Figure 6.

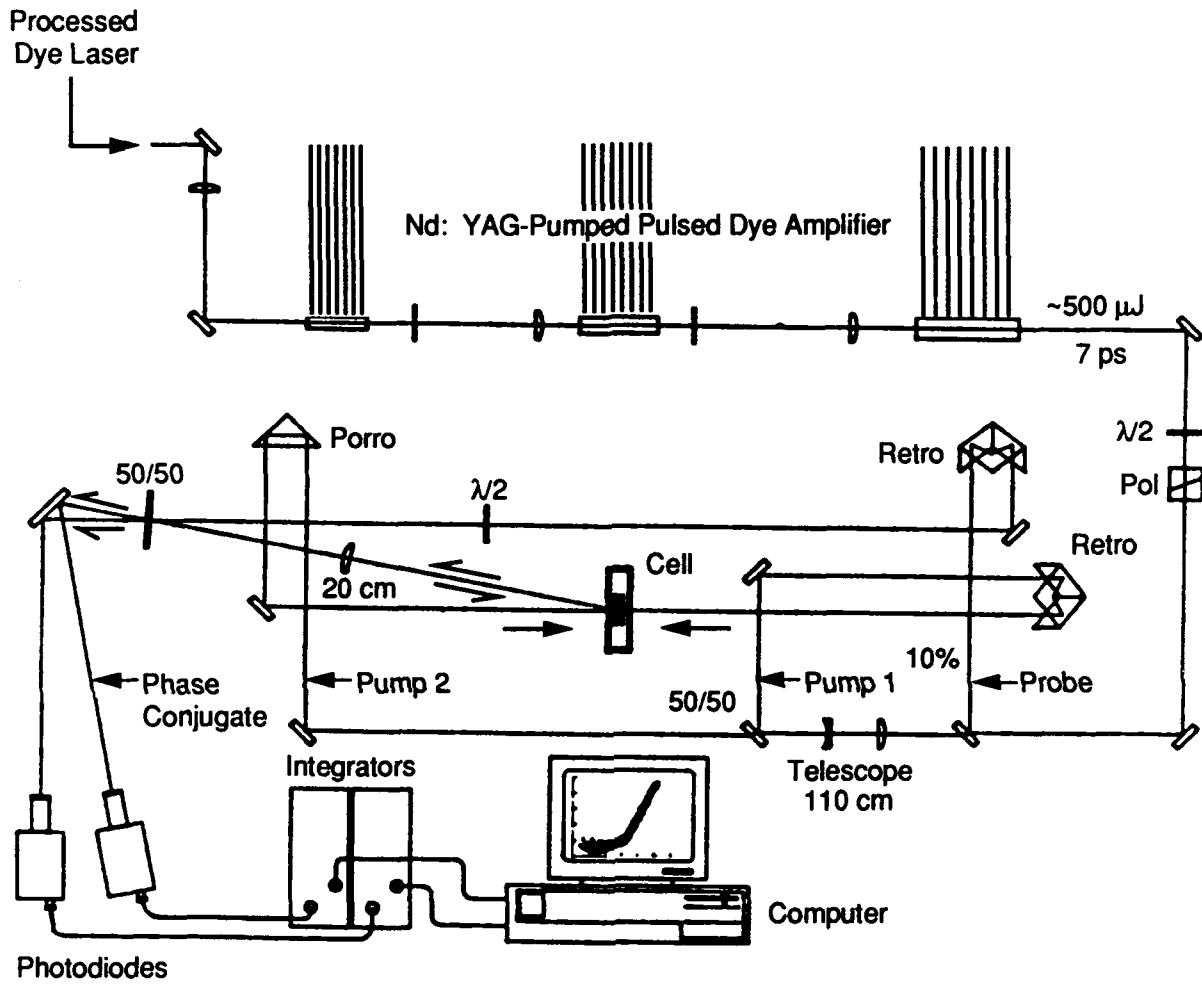
A combination of a half-wave plate and a Glan polarizer is used to define the polarization and power of the laser beam delivered from the pulsed dye amplifier. The beam is split into two pump beams that counterpropagate through the material contained in the quartz cell. A weak (typically 10%) probe beam with polarization perpendicular to that of the pump beams is directed at a small angle into the region illuminated by the pump beams. The phase-conjugate beam is produced antiparallel with the probe beam, and a portion of each beam is monitored on a shot-to-shot basis with calibrated photodiodes. A typical example for the signal-to-noise level that can be achieved is shown in Figure 7, which gives the phase-conjugate signal as a function of the probe intensity on a log-log scale. The slope of 3 indicates the order of nonlinearity of the DFWM process. The temporal response of the medium is monitored by varying the delay time between the pump and between the probe and pump pulses, which is done using computer controlled stepping motors that drive the retroreflectors in Figure 6.

The experimental sample used for generating Figure 7 is a novel high-temperature porphyrine based polymer that was developed in another laboratory at SRI. We have measured the third-order nonlinear susceptibility of this polymer, as well as of a range of solvents, as a first calibration procedure of the DFWM setup.

SURFACE ANALYSIS USING VERY INTENSE LASER LIGHT

Surface analysis by laser ionization (SALI), a technology developed recently at SRI for the chemical analysis of surfaces, uses nonresonant multiphoton ionization (NRMPI)¹¹ and offers a unique capability of sensitivity and quantitation. SALI's growing importance as an analytical tool is reflected in its recent commercialization by Perkin-Elmer Corporation. In practice, typically an ion beam sputters atoms and molecules from a surface under vacuum and the sputtered flux, predominantly neutral in charge, is photoionized by NRMPI. In the past, a standard excimer laser or common nanosecond Nd:YAG system operating at 266 nm was used for photoionization, delivering about 10^{10} W/cm².

A long-standing difficulty with these common lasers has been their very inefficient photoionization of atoms with high ionization potentials (because 3 or 4 photons are required with these UV wavelengths), which results in losses in sensitivity and quantitative ability. For example, the oxygen content of thin corrosion passivation films has been difficult to quantify. Much higher intensities are required to efficiently ionize oxygen atoms by NRMPI.



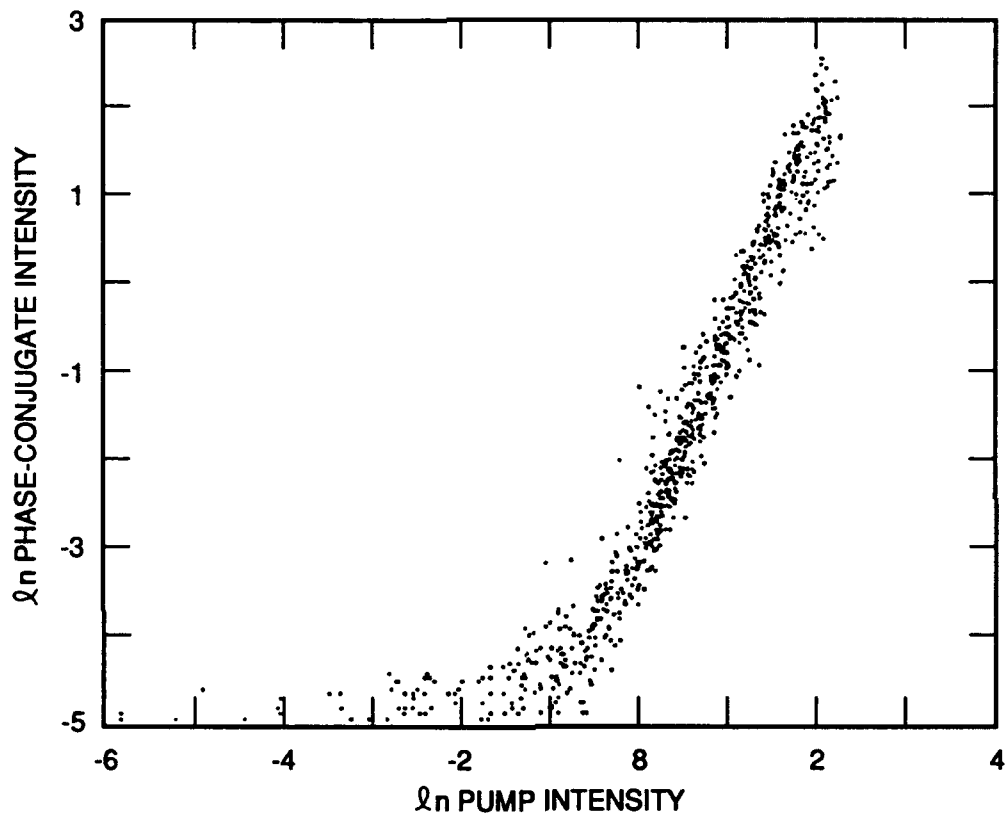
Photodiodes

NOTE:

Experimental set-up for optical phase conjugation by degenerate four-wave mixing in polymers.

RM-5541-1A

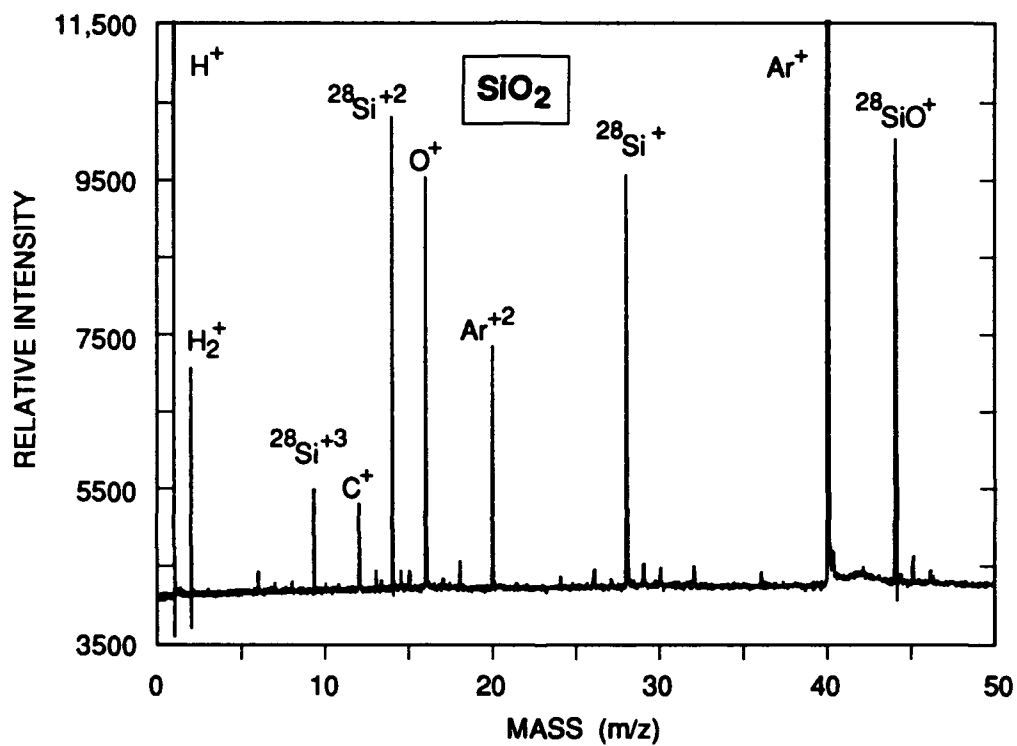
Figure 6. Layout of four-wave experiment used to measure third-order nonlinear susceptibilities in liquid and polymers.



RM-5541-4A

Figure 7. Typical phase-conjugate signal as a function of laser intensity (6350 Å, 2-ps pulse length.)

However, the high intensities needed have been achieved with our picosecond laser system which delivers about 10^{14}W/cm^2 for such SALI experiments. As a demonstration, numerous inorganic samples were examined, including SiO_2 from a 600-Å SiO_2 layer on Si (shown in Figure 8). The stoichiometry from the raw data is actually fairly good, reflecting a correction factor of roughly 4 for Si relative to O. Even though the O is efficiently ionized here, this higher sensitivity for Si is easily accounted for by differences in the effective ionization volumes, because Si is readily ionized and therefore the wings of the laser beam are more effective. Such effects are readily accounted for to make data from unknowns highly quantitative. Also, note in Figure 7 the presence of Si^{+3} and a modest amount of Ar^{+3} at m/z 13.3. The Ar is from the gas discharge ion gun used, and H_2 is a background gas in the vacuum chamber.



CM-330581-7

Figure 8. Time-of-flight mass spectrum from photoionization of neutral component released from SiO₂ substrate following ion bombardment. (6400Å, 500 fs, 1 × 10¹⁴ W/cm²).

PUBLICATIONS AND PRESENTATIONS

1. On the Wavelength Dependence of Multiphoton Ionization by Short-Pulse High Intensity Lasers. H. Helm, H. Bissantz, and M. J. Dyer. Presented at Symposium on Atomic and Surface Physics, Obertraun, Austria—February 1990.
2. Axicon Amplification of a Synchronously-Pumped Sub-Picosecond Dye Laser. M. J. Dyer, H. Helm. *Optics Lett.* Submitted for publication May 1991, see Appendix A.
3. Wavelength Dependent Resonant Multiphoton Ionization in Intense Laser Fields. H. Helm, M. J. Dyer, and H. Bissantz. Presented at DAMOP meeting (1990), Monterey, CA.
4. Giant Stark Shifts in Picosecond Photoionization. H. Helm, M. J. Dyer, and H. Bissantz. Submitted to *Phys. Rev. A.* for publication (May 1991, see Appendix B).
5. Wavelength Dependent Multiphoton Processes in Xe and H₂ in Intense Laser Fields. H. Helm, M. J. Dyer, and H. Bissantz. Presented at International Conference on Multiphoton Processes, ICOMP V, Paris, France, September 1990. Book of Abstracts, p. 160.
6. Dissociation of H₂ in Intense Laser Fields. H. Helm. Presented at Third U.S.-Mexico Atomic and Molecular Physics Symposium, Cocoyoc, Mexico, March 1991; published in *Few Body Problems*, T. Morgan, Ed. (World Scientific Publishing Co., London, 1991).
7. Photodissociation During Photoionization of H₂ in Strong Laser Fields. H. Helm. Invited lecture at NATO Workshop on Coherence Phenomena in Atoms and Molecules in Laser Fields, Hamilton, Canada, May 1991; published in *Coherence Phenomena*, A. D. Bandrauk, Ed. (Plenum Press, New York, 1991).
8. Dynamics of Half-Collisions in Intense Laser Fields. H. Helm. XVII International Conference on the Physics of Electronic Atomic Collisions, Brisbane, Australia, July 1991.
9. Multiphoton Excitation of H₂ in Intense Laser Fields. H. Helm. Invited lecture at Conference on Quantum Electronic and Laser Science, Baltimore, MD, May 1991.
10. Photodissociation during Photoionization of H₂ in Intense Laser Fields. H. Helm, M. J. Dyer, H. Bissantz, and D. L. Huestis, submitted to *Phys. Rev. A.*, May 1991, see Appendix C.
11. C. H. Becker and K. T. Gillen, *Anal. Chem.* **56**, 1671 (1984).

PROJECT SUMMARY

PRINCIPAL INVESTIGATOR: Dr. Hanspeter Helm
Molecular Physics Laboratory
SRI International
Menlo Park, CA 94025

INCLUSIVE DATES: 15 February 1988 - 15 February 1991

CONTRACT NUMBER: F49620-88-K-0006

COSTS and FY SOURCE: \$ 455,066 FY88/91

PERSONNEL: Hanspeter Helm, Program Manager
Christopher H. Becker, Group Leader
Christian Bordas, Postdoctoral Fellow
Holger Bissantz, SRI International Fellow
Richard A. Copeland, Physicist
Mark J. Dyer, Physics Associate
David L. Huestis, Associate Director
Ravinder Kachru, Senior Physicist

REFERENCES

1. D. S. Bethune, *Appl. Optics*, **20**, 1897 (1981).
2. W. J. Tomlinson, R. H. Stolen, and C. V. Shank, *J. Opt. Soc. Am. B* **1**, 139 (1984).
3. T. J. McIlrath, R. R. Freeman, W. E. Cooke, and L. D. van Woerkom, *Phys. Rev. A* **40**, 2770 (1989).
4. P. Agostini, J. Kupersztych, L. A. Lompre, G. Petite, and F. Yergeau, *Phys. Rev. A* **36**, 4111 (1987).
5. M. D. Perry, A. Szoke, and K. C. Kulander, *Phys. Rev. Lett.* **63**, 1058 (1989).
6. G. Alber, H. Ritsch, and P. Zoller, *Phys. Rev. A* **34**, 1058, (1986).
7. H. Helm, *Phys. Review A* **38**, 3425 (1988).
8. J. F. Reintjes, *Nonlinear Optical Parametric Processes in Liquids and Gases* (Academic, Orlando, Fla, 1984), p. 327.
9. C. H. Becker and K. T. Gillen, *Anal. Chem.* **56**, 1671 (1984).

Appendix A

**AXICON AMPLIFICATION OF A SYNCHRONOUSLY-PUMPED
SUB-PICOSECOND DYE LASER**

Axicon Amplification
of a Synchronously-Pumped Sub-Picosecond Dye Laser

M.J. Dyer and H. Helm
SRI International
333 Ravenswood Avenue
Menlo Park, CA 94025

Abstract

The performance of a conical axicon dye amplifier pumped by a frequency-doubled Q-switched Nd:YAG laser is evaluated. The open aluminum axicon described here forms a relatively inexpensive power amplification stage capable of routinely delivering pulse energies of several millijoules in under 1 ps from DCM over wavelengths between 610 and 660 nm. Measurements of the transverse mode quality indicate near-diffraction limited performance for maximum focusability.

INTRODUCTION

The use of multiple-stage amplification schemes¹⁻³ has been widely applied to raise the low energy, short pulses produced by sync-pumped and colliding-pulse dye lasers to microjoule levels. In schemes where concentrated pump laser beams and dye solutions are used, phase perturbations across an initially well-behaved wavefront due to high intensities can occur within short time scales. Specifically, in the final stage of high gain-saturated amplification, phase front distortions limit the ultimate intensities which may be reached through focussing. Therefore it is desirable to introduce to the final amplifier a beam as large as possible while avoiding hot spots from uneven pump geometries. Axicon amplifiers permit amplification

of large beams while avoiding beam distorting effects on nanosecond and femtosecond pulses, as demonstrated by Kuhnle⁴ and Wood⁵, respectively. Additionally, the conical geometry of the axicon is particularly well-suited to pumping by doughnut-mode lasers, and may be easily and economically upscaled in size for higher power applications. The currently published designs, however, suffer from an important drawback, namely a singularity in the pump intensity at the axicon center. This singularity leads to undesirable generation of an intense amplified spontaneous emission (ASE) spike.

The main emphasis in this paper is to describe an axicon design that both avoids this ASE problem and addresses the problem of radially-even dye flow conditions to minimize beam distortion from liquid turbulence. This new design has been tested for pump-energies up to 500 mJ and is also fairly inexpensive, an important consideration in scaling axicon reflectors for larger beam geometries.

AXICON DESIGN

To optimize the clean amplification of high-power subpicosecond pulses we have developed an open axicon design that incorporates several essential features not investigated before.⁴⁻⁶ A diagram of the axicon amplifier is shown in Fig. 1. To avoid intensity-driven self-phase modulation effects, the size and design were chosen to accommodate as large a dye laser beam as possible, given our practical constraints of 1" clear aperture beam-line optics, doubling crystals and vacuum access ports. Also, a large area of the axicon's reflector meant that high pump energies could be introduced without the danger of exceeding the damage threshold of uncoated aluminum.

The reflector was machined from a 10" diameter, 2" thick disk of Alcoa type 7075-T6 small-grain aluminum, the dye cell mounting plate and window hardware from stainless steel, and all other components from standard aluminum. Dimensions of the reflector were tailored to a doughnut-shaped beam profile with roughly 7.5 cm inner and a 17.5 cm outer diameters at $1/e^2$ intensities. The reflector's surface was polished "in-house" on a lathe in four steps, finishing with a 0.5 micron alumina suspension that produced an average reflectivity of ~85%. The glass dye cell measured 2.5 cm outside diameter by 6 cm in length and was mounted in the center of the axicon with three 1 mm diameter rods threaded at either end. Both windows were AR-coated for reduced ASE and maximum transmission.

Critical to minimizing refractive index changes across the diameter of the amplified beam was the smooth introduction and flow of the liquid dye through the window mounts and across the cell. Initial designs neglected the effects of a turbulent flow, and subsequent observations of the unamplified dye laser beam through a spatial filter revealed wildly fluctuating transmissions which were dependent on flow rate. New mounts were constructed which smoothly distributed liquid dye around the circumference before injection into the dye cell volume. Additionally, the inlet "ring" was relieved and polished to permit the liquid to gradually expand into the gain region, thus minimizing changes in the index within the active volume and reducing the potential for turbulent flow evolution. Spatial filter analyses were then repeated to show that the mode fluctuations had dropped dramatically to produce under 5% peak-peak transmission variations under flow rates of ~5 l/min. This liquid inlet design⁷ is shown in Figure 2.

The amplifier was optically pumped by splitting the 450 mJ 532 nm output from a Quanta-Ray DCR-II doughnut-mode laser; 150 mJ was reserved for the transversely-pumped, triple-stage Bethune⁸ prism amplifiers, and the remainder directed into the axicon. The pump beam was expanded through a -6 cm lens onto a 23 cm diameter, 75 cm fl aluminum-coated telescope mirror, where it was collimated and sent back toward the axicon. The large central hole in the beam permitted clear passage around the optics and mounts, with the exception of 5 mm diameter posts which were positioned in-line with the dye feed tube. The total pump energy reaching the dye cell was 220 mJ, and due to the large size of the pump beam at the telescope and axicon reflectors, peak intensities never reached beyond 0.5 MW/cm^2 on the reflectors, well below the damage threshold for unprotected aluminum. Optimal dye absorptions at 532 nm varied from 0.9 to 1.2 cm^{-1} (.022 - .030 g/l) depending upon the wavelength under amplification, and total output exhibited a fairly broad dependence on concentration with ASE increasing at higher concentrations.

The output of a synchronously-pumped dye laser operating on DCM was amplified to ~ 400 μJ by the three prism amplifiers and expanded to 1.75 cm ($1/e^2$) diameter before delivery into the axicon. Two beam configurations were investigated. In single-pass, the dye beam was directed from the back of the amplifier and picked off by a 45° reflector. Single-pass typically yielded 1.5-2 mJ for 250 mJ pump, increasing the energy from the triple-stage by roughly a factor of five. The double-pass geometry, shown in Fig. 1, was accomplished by retroreflecting the single-pass amplified beam immediately back through the axicon, and using a polarizer/quarter waveplate combination, in addition to about 2 meters of path/time distance to isolate the triple-pass

amplifier from the backward-travelling pulse, and couple out the amplified beam. Pulse energies exceeding 4 mJ in 2 picoseconds over a wavelength range from 610 to 660 nm were readily attained in this geometry. Also, frequency doubling in KDP yielded conversion efficiencies averaging 25% and energies of over 1 mJ/pulse at 320 nm.

Although the net energies available from this device were initially impressive, a fairly large ASE component complicated the determination of the output energies and analysis of amplified beam spatial profiles. Attempts to reduce the accumulated ASE from the earlier amplifier stages met with reserved success. Spatially filtering between stages improved the isolation from ASE produced by the earlier stages, but nothing removed the ASE primarily generated by the axicon amplifier.

In order to better diagnose and optimise the spatial characteristics of the gain produced by the axicon, the gain profiles were measured using near- and far-field optical configurations for imaging with a Beamcode beam profiling package. Fluorescence profiles taken of the pumped volume with a two-dimensional CCD array reflected the convolution of a radial dependence and the logarithmic absorption of the pump by the dye, close to the theoretically expected form of a cylindrically uniform radial flux into an absorbing medium:

$$I = I_{R_0} R^{-1} (e^{+c(R-R_0)} + e^{-c(R+R_0)}) \quad (1)$$

where R is the radial position from the axicon center, R_0 is the diameter of the dye-flow cell and I_{R_0} is the pump intensity at the perimeter of the dye cell and c is the linear absorption coefficient.

For dye concentrations producing at least 25% of optimum amplification, these data revealed a strong superfluorescent central spike (as predicted by the singularity in equation (1)). This spike contributed a significant ASE component to the overall energies and damaged the amplifier's input window, as well as some of the optics located up- and downstream. Only when the concentrations were high enough to strongly absorb the most of the pump within a few millimeters of the dye cell wall was the spike sufficiently attenuated. This, however is undesirable because the center of the dye volume is then left virtually unpumped.

The successful method of smoothing the gain profile, as suggested by Wood⁵, involved sandblasting the dye cell to an evenly diffusive white finish. The outer surface was selected because roughening the inner surface did little

to diffuse a significant fraction of the pump light, and causes greater drag on the flow, thus raising the potential for deposit formation and damage. Fluorescence profiles taken following this modification revealed that the gain profile was homogenized tremendously. The total pump intensity reaching the dye was reduced only slightly by ~8%, as determined from transmission measurements on glass disk diffuser with a Scientech laser calorimeter. Figure 3a,b illustrate the differences observed in fluorescence for the two configurations. Overall, no decrease in total energy extraction was observed, and the diffusely-coupled pump produced an amplified beam with near-negligible ASE (~5%). Since the ASE energy measured was integrated over the 10 ns envelope of the Nd:YAG pump laser, while the energy contained in the amplified sync-pumped dye lasts only 10^{-4} times as long, the intensity of the amplified spontaneous emission compared with the short pulse intensity was effectively negligible, and therefore, techniques to reduce ASE further were not pursued.

Illustrated in figure 4 are three-dimensional maps of the dye beam spatial mode after passage through the axicon unamplified (a) and amplified (b). As expected, the profile exhibits a slight narrowing of the gaussian input beam due to the higher gain at the center of the radially pumped cell; however, the ASE spike is virtually eliminated. One would anticipate that this technique of close-coupled diffusive "spoiling" of the pump beam could be tailored further to reduce this narrowing with little loss in efficiency.

PERFORMANCE TESTS

Measurements of the gain integrated over the entire spatial modes of the input and output beams were made of the axicon amplifier on a single-shot basis with pyroelectric energy probes as the input energy was varied using a half-waveplate, polarizer combination. The results of this are shown in Figure 5a. As illustrated, saturation appeared to occur at roughly 300 microjoules for a pump energy of 220 mJ. For the maximum dye input, the Nd:YAG source into the axicon was also varied in energy to determine if pump saturation appeared as a roll-off in the gain versus pump energy. As shown in Figure 5b, no saturation was seen for our pump laser, leading us to the conclusion that this amplifier could handle even larger pump sources for greater dye laser energy yields. As a demonstration of this, a second Nd:YAG source was installed in parallel, allowing pump energies into the axicon up to 700 mJ. The pump beams were propagated side-by-side on the optics leading up to the axicon and overlap of both beams on the dye cell was easily

accomplished without any loss of pumping symmetry. Increased timing jitter between the two pump lasers and the sync-pumped dye laser led to a more unstable output, but peak energies were found to reach past 6 mJ for this pumping scheme.

In order to determine the focusability of the amplified beam, we attenuated the output by reflecting off several quartz flats and focussed it through a spatial filter, varying only the size of the pinholes used at the focus. The filtered beam energy was then measured and profile observed with an CCD array. This provided a direct measurement of the spot size and coupled with a temporal profile taken with an autocorrelator, we found the peak intensity to be greater than 10^{15} W/cm² when focussed with a 12.2 cm "best-form" lens.

Extending this technique to shorter pulses was straightforward. The decision to frequency-chirp and grating-compress the output of the 78 MHz sync-pumped dye oscillator was made in order to preserve the tunability of the dye laser system. To achieve this, the 2.5 ps, 300 mW output of the dye oscillator was first passed through a Faraday isolator, then coupled in and out of a 7 meter long polarization-preserving, single-mode fiber (Newport) using 20X microscope objectives. This broadened the spectral envelope from 6 Å to > 20 Å, and lengthened the temporal width to 30 ps. These pulses were then compressed in a double-pass off a 2400 lines/mm holographic Littrow grating (American Holographic) and 5 mm retro-reflecting prism positioned to allow approximately 2.7 cm between grating bounces. Pulses of 300 femtoseconds and 0.6 nJ exiting the compressor were then fed into the amplifiers. Total gain on these pulses reached $5 \cdot 10^6$, producing pulse energies averaging 3 mJ. Although passage through the amplifiers did impose an additional chirp, the pulse could be narrowed by adjusting the cavity length of the sync-pumped dye laser to compensate slightly. Measurements with a single-shot autocorrelator of the amplified compressed pulses indicated that after compensation, the widths at half-maximum remained on average below 1 picosecond.

In conclusion, we have demonstrated a large aperture, axially-pumped amplifier stage for the production of short, high energy pulses. The open axicon design is well-suited for high power doughnut-mode pumping, allows for optimal diffusive coupling of the pump beam into the dye medium, and serves to overcome the cost restrictions of scaling up all-glass conical reflectors. In scaling gain volume to reduce potential wavefront perturbations due to high intensities, we have also addressed the issue of turbulent dye flow, and the

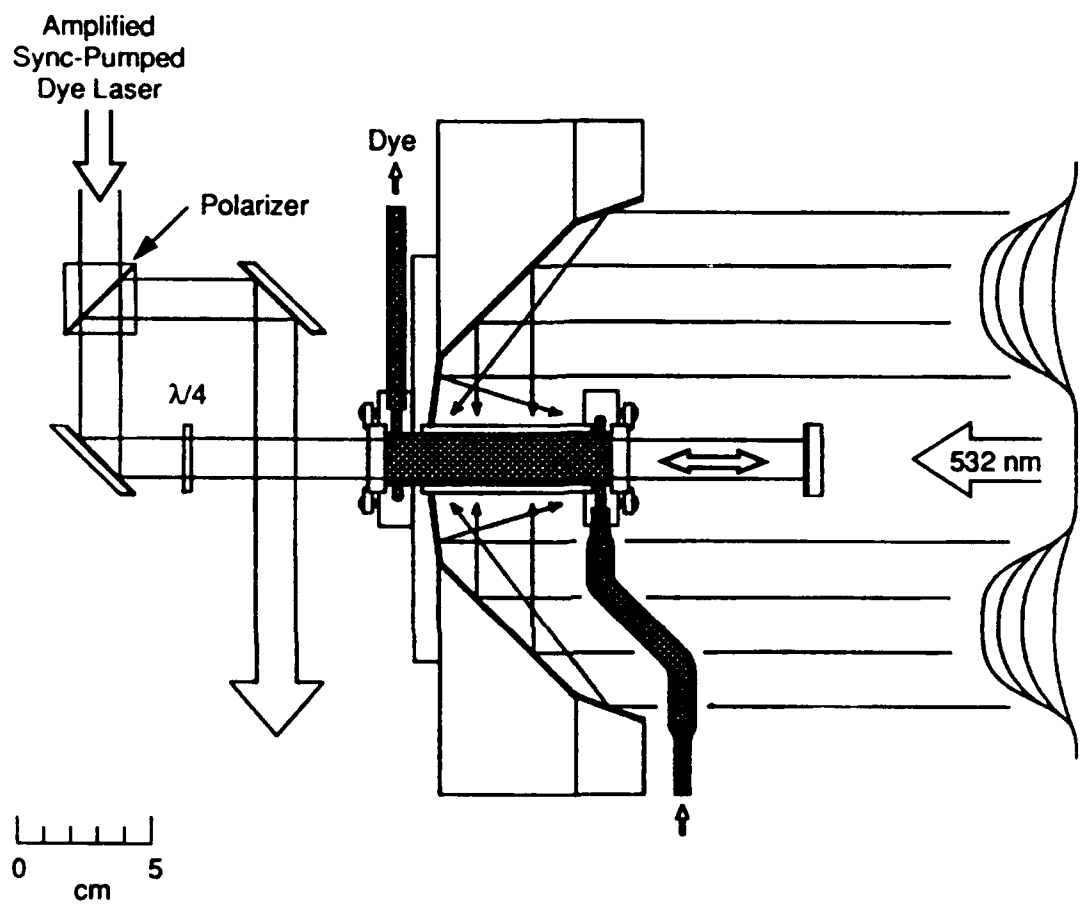
feasibility of combining multiple pump sources was demonstrated to illustrate the potential for even greater energy yields.

ACKNOWLEDGEMENTS

This research was supported by the Air Force Office of Scientific Research under Contract No. F49620-88-K-0006.

REFERENCES

1. R. L. Fork, C. V. Shank, and R. T. Yen, Appl. Phys. Lett. 41, 223 (1982).
2. C. Rolland, and P. B. Corkum, Opt. Comm. 59, 64 (1986).
3. Y. Ishida, T. Tokizaki, and T. Yajima, Opt. Comm. 68, 295 (1988).
4. G. Kuhnle, G. Marowsky, and G.A. Reider, Appl. Opt. (to be published)
5. W.M. Wood, G. Focht, and M.C. Downer, Opt. Lett. 13, 985 (1988).
6. F. P. Schäfer, Appl Phys. B. 39, 1 (1986).
7. Design drawings are available upon request from the authors.
8. D. S. Bethune, Appl. Opti. 20, 1897 (1981).



RM-5541-7

Figure 1 Cut-away of axicon amplifier and optical paths of the pump and dye laser in a double-pass configuration.
 The clear diameter of this stage is 22 mm.

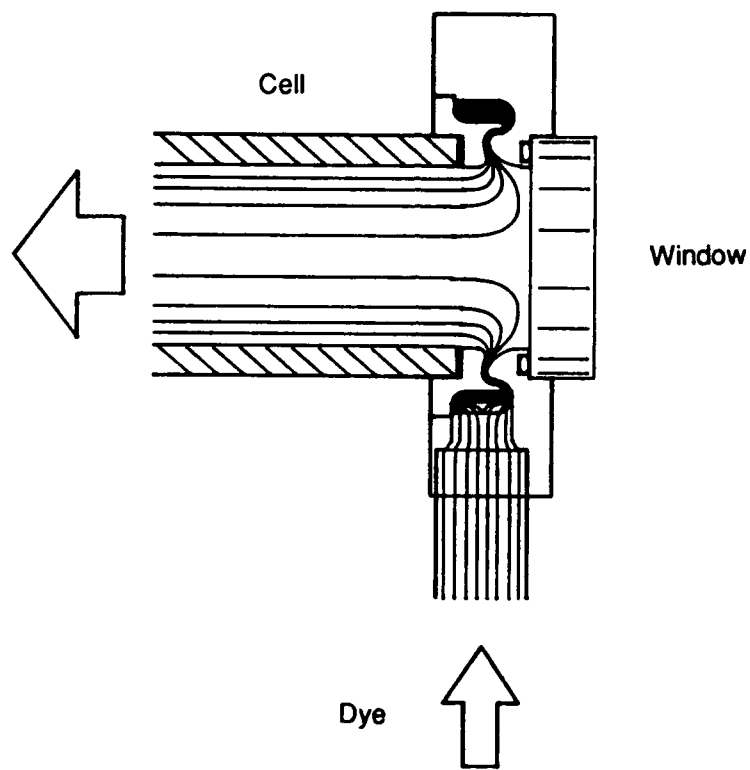


Figure 2 Cut-Away of dye injection port into amplifier cell.

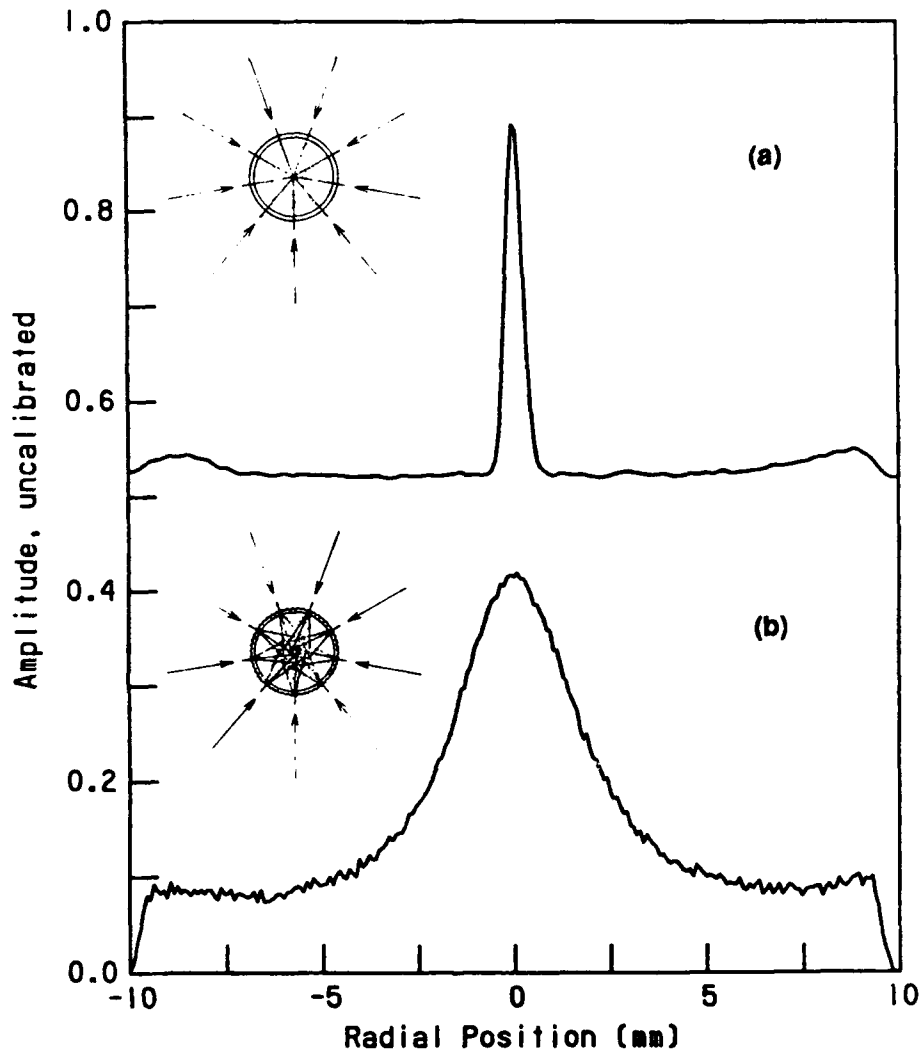
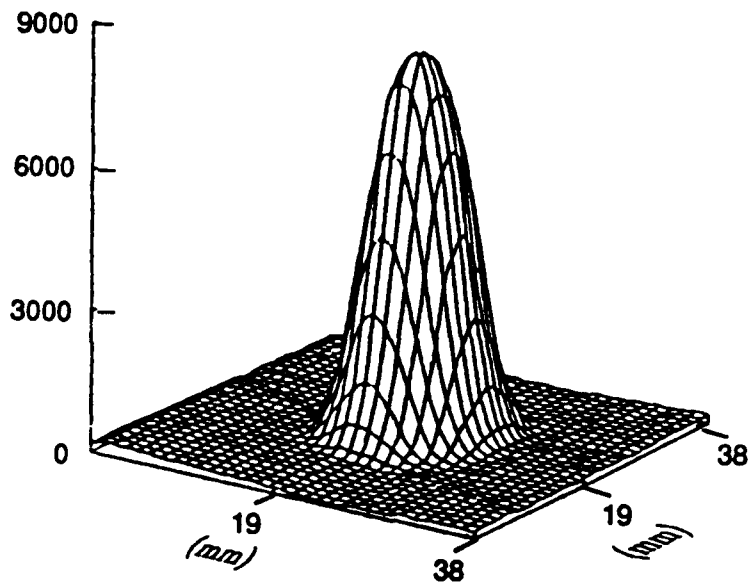
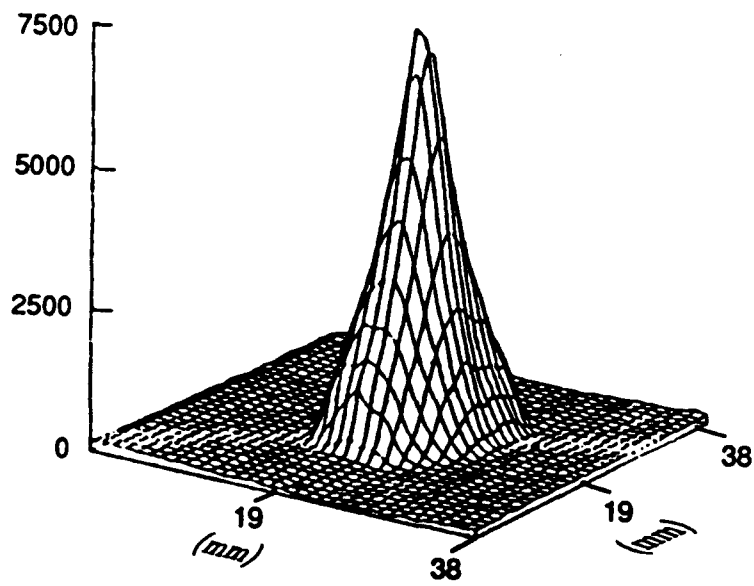


Figure 3 Spatial distribution of end-on fluorescence from the dye gain volume for the (a) conventional axicon, and (b) axicon with diffused pumping.



(a) After pulse compression



(b) After full amplification

RA-5541-010

Figure 4. Measured laser beam profile.

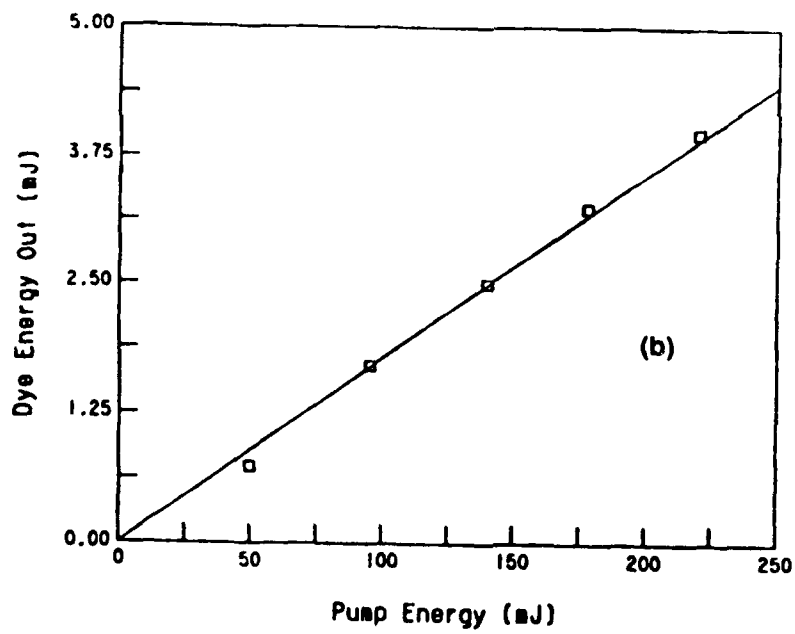
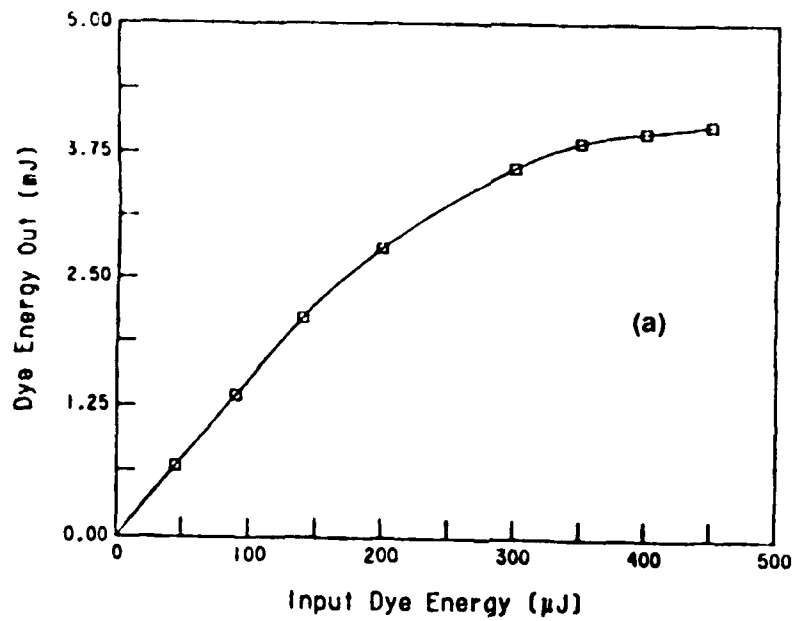


Figure 5 Integrated gain (a) as a function of dye laser input energy into the axicon and (b) as a function of pump energy.

Appendix B

GIANT STARK SHIFTS IN PICOSECOND PHOTOIONIZATION

GIANT STARK SHIFTS IN PICOSECOND PHOTOIONIZATION

H. Helm, M. J. Dyer, and H. Bissantz
Molecular Physics Laboratory
SRI International, Menlo Park, Ca 94025

ABSTRACT

We report photoelectron energy spectra from seven-photon ionization of xenon using pulse-lengths of 2 ps and peak intensities from 10 to 120 TW/cm². The spectra appear structured, showing very large ac-stark shifts following resonance enhanced multiphoton ionization. Shifts up to 1 eV are observed for 7p state resonances and up to 2 eV for 6p state resonances. The resonance structures are also resolved in above-threshold ionization photoelectron peaks.

MP 90-165
September 7, 1990

The recent discovery of substructures in the photoelectron energy spectra recorded with subpicosecond laser pulses shows that n-photon ionization can proceed efficiently^{1,2} at intensities at which an excited atomic state is shifted into resonance with the (n-1)photon dressed ground state of the atom. The initial observations of substructure by Freeman et al² have been confirmed by work of the groups of Agostini³ and of Feldman⁴ and they are predicted in recent theoretical work.^{5,6} A simple interpretation uses the following key ideas: In an intense electromagnetic field all atomic energy levels can experience significant ac-Stark shifts prior to ionization. The up-shifting of the ionization limit arises primarily from the quiver energy, ϵ_p , that the free electron acquires in the em-field. The shifts of the continuum and of the highly excited states of the atom are generally much stronger than those of the ground state level of either the neutral or the ion⁷ which we neglect in the following discussion. In such a situation, a dynamic resonance may arise at a specific intensity at which an excited level becomes resonant with the neutral ground state dressed by an integer number of photons. At this intensity, I_r , the photoionization probability can be strongly enhanced over the purely nonresonant process, giving rise to an electron with drift energy

$$E_d = N h\nu - E_i - \epsilon_p(I_r) \quad (1)$$

where E_i is the unperturbed ionization potential and I_r is the local intensity at which the ionization process occurs. Several such resonances can be encountered within a single laser pulse owing to the temporal and spatial distribution of intensity. In the case that a temporally short laser pulse is used the photoelectron finds insufficient time to "surf" off the focal volume⁸ and thereby convert the quiver energy into drift energy. Without this "ponderomotive scattering"⁸ the photoelectron appears at the detector with an energy given by (1), revealing the resonance induced by the Stark effect at intensity I_r .

In the current paper we report observations of these effects, however using a laser with pulse length of ~ 2 ps. The specific case investigated is seven- to ten-photon ionization of xenon involving six-photon Stark-induced resonances. Substructure in the photoelectron spectra appears readily at this pulse length. Some differences are noted in comparison to previous work.^{1,2,3,9,10} These are possibly due to different pulse lengths and peak intensities.

The photoelectron spectra are recorded in a magnetic bottle, time-of-flight spectrometer that uses permanent magnets.¹¹ Photoelectrons are detected on a multichannel plate at the end of a 64 cm drift distance. The electron signal is monitored by a constant fraction discriminator whose output feeds a chain of time-to-digital converters, each with 1-ns resolution. Up to sixteen electrons can be recorded per laser shot and the pressure in the ionization region is adjusted (between 1×10^{-8} and 1×10^{-6} Torr) to ensure that the number of photoelectrons remains below this limit. In low-intensity, resonant ionization of H_2 we have demonstrated a resolution of 50 meV at 1 eV electron energy using this device.¹²

The home-built laser uses DCM-dye in an optically flat sapphire jet which is synchronously pumped by a mode-locked frequency doubled YAG (1.6 W) at 78 MHz. A two-plate birefringent filter permits tuning over the range from 610 to 660 nm at pulse lengths of ~ 2 ps. The dye-laser output mirror has a transmission of 30%, yielding 400 mW at 620 and 650 nm. The mode-locked laser is synchronized with a 10 Hz, frequency doubled Yag laser (450 mJ) that pumps four amplifier stages. The first three stages are Bethune prism amplifiers¹¹ with 1 mm, 3 mm, and 6 mm bore diameter. An amplification to 500 μ J is typically achieved in these three stages. The fourth stage is an open axicon amplifier¹² using a 25-mm diameter dye-cell (length 70 mm). The dye beam is telescoped to a diameter of 2 cm and boosted to 4 mJ in double-passing the axicon. In order to be able to enter the narrow aperture into the magnetic bottle the laser beam is collimated to 1 cm diameter after the axicon and focused into the center of the spectrometer using a 15-cm lens. Based on the near gaussian and diffraction limited beam profile¹² we estimate that the focal diameter ($1/e^2$) to be around 14 μ m although a direct measurement of the focal properties at full

power have not yet been carried out. Intensities quoted below are lower limits, averaged over a conservatively chosen 20 μm spot diameter using a 2 ps envelope, obtained from autocorrelation measurements assuming a sech^2 pulse shape.

A close-up view of the seven-photon substructure observed in the photoelectron spectrum at 620 nm is shown in Figure 1. To record this spectrum the laser pulse energy was held to 200 μJ corresponding to an average peak intensity exceeding $3 \times 10^{13} \text{ W/cm}^2$. Two clear substructures appear in this spectrum, shifted down in energy from the seven-photon energy limit, $E_7 = 7 \text{ h}\nu - E_i$. Here E_i is the energy of the lowest ionization limit of Xenon, $\text{Xe}(2\text{P}_{3/2})$. While we consider the absolute energy scale to be only precise to approximately 100 meV, (from calibration measurements using nanosecond pulse multiphoton ionization), the relative separation between the two peaks is very accurately 0.31 eV, approximately the zero-field separation between the 4f and 5f manifolds of xenon.¹³ Also the shift of either peak from the position of the nonresonant seven photon ionization process is closely equal to positions predicted by Equation (1), under the assumption that these states have ac-Stark shifts equal to the quiver energy. We therefore assign these peaks to the Stark-shifted resonances 4f and 5f. This identification is in accordance with that in previous work although only weak evidence is found for contributions from the 8p level, and higher states, which appeared with significant intensity in some spectra of previous work.^{1,3} The magnitude of the ponderomotive energy calculated for this laser energy (1.1 eV at $3 \times 10^{13} \text{ W/cm}^2$) is certainly sufficient to account for the observed shifts.

In Figure 1 the observed photoelectrons are collected into 2 meV wide energy bins and their number is normalized to the chamber pressure and the number of laser shots. In order to indicate the statistical significance of individual features we also quote respective absolute numbers: At the peak of the feature assigned to 4f a total of 160 electrons per 2 meV bin were recorded in a run where 14,000 laser shots fell within the specified laser energy. This means that of the structures in Figure 1 only the two main peaks, labeled 4f and 5f bear statistical significance. Also, the electrons shown in Figure 1 represent only about 10% of the total number of electrons detected in

this run (18,000 electrons). The remaining electrons are distributed over above-threshold ionization (ATI) peaks, some of which are shown in the lower trace in Figure 2. We recognize similarly shifted resonance structures, corresponding to 4f and 5f that appear at this intensity in the first and second ATI interval, that is for 8-hv and 9-hv ionization, while again, no electrons appear at the nonresonant multiphoton energies.

Figure 2 further shows the development of peak structures with intensity. As the intensity is raised two modifications appear in the spectra: For one, a strong population shift into the higher ATI peaks occurs. Secondly, an intensity switching towards peaks at lower energy occurs within each n-photon interval. To a first approximation this switching of intensity from one resonance peak to the neighbor is not accompanied by a continuous shift of the resonance position. Switching of the resonance peaks with intensity has previously been observed by Agostini et al.¹⁴

The switching reveals that at higher intensity resonances that are further separated from the zero field six-photon energy can be forced into resonance. We see that the 5f subpeak apparently disappears in the 7-hv spectrum as the intensity grows. At least one new peak appears for the 8-hv spectrum as the intensity increases. This peak becomes the prominent feature for the nine-photon case and it lies just below the position marked 7p. At yet higher intensity (top trace in Figure 2, $I > 1.2 \cdot 10^{14} \text{ W/cm}^2$) this trend continues with an additional peak appearing (marked by arrows). Higher intensities were not investigated in order to avoid complications from background photoionization. The background pressure is $\sim 1.5 \cdot 10^{-8}$ torr, however no background subtraction is required at the intensities used here.

Each of the three traces shown in Figure 2 is taken from a run where $\sim 18,000$ electrons were collected at the specified laser energy. The energy bins into which the counts are distributed are 20 meV wide in Figure 2. In order to compare the three traces on a normalized scale (electrons/shot Torr) the curves have to be multiplied by the factors quoted in Figure 2. On the scale in Figure 2 the 5f peak in the seven-photon spectrum decreases as the intensity grows. However when accounting for the normalization factors we see that the the height of the 5f peak

rises by a factor of 15 when going from 200 to 400 μJ . It rises however less than the 4f feature in the 8-photon spectrum, and both are dwarfed by the new feature which switches in between 200 and 400 μJ and shows up with relatively higher importance in the higher ATI peaks. These rather complex partial photoionization rates inherently reflect the ratio of rates for six-photon excitation of the ground state to (n-6) photon ionization of the Stark-shifted state.

Similar observations were made at 650 nm. Typical results are presented in Figure 3. For a wavelength of 650 nm the six-photon energy is just below the unshifted 8p levels of xenon. The 4f peak is thus the first peak that could be shifted into resonance (provided that all levels shift up in energy), and it is the only feature appearing in the low-intensity seven-photon spectrum. We note that this peak has a sharp leading edge at the higher energy end, in contrast to the 4f peak at 620 nm. This may in fact indicate that the width of the 4f peak observed actually reflects the ionization dynamics rather than the apparatus resolution. The 4f level is only within 450 meV from the six-photon resonance energy at 650 nm. Provided this level shifts like the free electron, the resonance condition is reached at intensities as low as $5 \times 10^{12} \text{ W/cm}^2$. At this low intensity the six-photon rate to drive the transition may be insufficient to efficiently drive the six-photon transition, causing the sharp cutoff of the peak at the higher energy end (corresponding to "lower" ac-Stark shift). We note that evidence for contributions from levels intermediate between 6p and 7p at higher intensity.

Provided the ac-Stark shifts of the excited states are independent of wavelength, the magnitude of the shifts as a function of wavelength should reflect the intensity dependence of the Stark shifts. On this basis, Agostini et al³ converted the shifts they observed at various wavelengths into a function of intensity.

An alternative presentation of experimental shifts which does not assume wavelength independence is used in Figure 4. This plot, inspired by Figure 3 of Potveligde and Shakeshaft⁵ shows the energy level diagram of the region of interest in xenon as a function of intensity, on a scale relative to the continuum shift. States which have ac Stark shifts equal to the quiver energy

appear in this plot as constant with intensity. Thus the six-photon dressed ground state level (the ac-stark shift of the ground state is neglected here) appears on a negative slope (full lines in Figure 4), falling with the quiver energy as the intensity grows. The quiver energy is given by¹⁶

$$\epsilon_p(\text{cm}^{-1}) = 750 I \lambda^2 \quad (2)$$

where I is the intensity in TW/cm^2 and λ is the wavelength in μm . In case that the ac-Stark shift of the ground state is negligible and that no ponderomotive scattering of electrons occurs then the photoelectron resonances observed at the energy E_d have to lie along the 6-photon curves, at an energy given by

$$E_r = E_i - E_d - (N-6) h\nu \quad (3).$$

The experimentally observed resonance features in 7, 8, and 9-photon ionization at various intensities are plotted in Figure 4 as the full squares.

Excited states with an ac-stark shift equal to that of the free electron appear constant with intensity in the representation chosen in Figure 4. We have indicated this situation for selected excited states by the thin lines. They merely serve as a guide to the eye. From the location of the experimental points it appears that the 4f states undergo shifts rather similar to that of the continuum. On the other hand a group of experimental point falls the 7p and above the 6p energies.

In general, shifts quite different from that of the free electron are expected for bound states from which other excited states can be reached in near resonance.⁵ In the case of xenon this is certainly expected for the 7p states. These connect at visible wavelengths to the autoionizing ns' and nd' members of the series converging to $\text{Xe}(2P_{1/2})$. A second-order Stark shift calculation for the $J = 0$ 7p level by Agostini et al.³ predict a rather strong wavelength dependence of its ac-Stark

shift. The results of these calculations at the two wavelengths used in this work are shown in Figure 4 by the open circles. The circles mark the positions where the $7p[0\frac{1}{2}]_0$ state is predicted³ to intersect the 620 and 650 nm curves. It is impossible to guess where the other J components would lie. Nevertheless, similar shifts (less than ponderomotive), may occur for the J = 2 states of 7p at this wavelength since the wavelengths used fall short in energy of pumping the 8d' resonance (see Figure 3 of Ref. 3). Calculations⁶ predict a much stronger role for J = 2 states in peak formation than for the J = 0 states. Another explanation for the peaks that fall intermediate between 6p and 7p could be to assume that they originate from ionization into $Xe(2P_{1/2})$. However, in this case no energy shift that is consistent for 620 and 650 nm results. A more realistic alternative may be to invoke a five-photon resonance with the Stark shifted 6s levels. At zero field these peaks are off resonance by 1.56 and 1.10 eV at 620 and 650 nm respectively. Since these peaks never show up in the 7-photon spectrum at least 3 additional photons were required to ionize these Stark-shifted intermediate. Very clearly, the experiment cannot guide us at this point to a definitive answer.

For the 6p states transitions to the $8d(2P_{3/2})$ bound levels are near resonant, and these may influence the ac-stark shift pattern. In addition, in order to Stark-shift the 6p-levels to the six-photon energy, the intensity has to rise above the threshold intensity at which the number of photons required to ionize $Xe(1S_0)$ increases from 7 to 8 photons. This threshold is 31 TW/cm² at 650 nm and 52 TW/cm² at 620 nm. It is therefore conceivable that a mixture of 6- and 7-photon resonances contribute to the peak that appear above the position of the 6p levels.

ACKNOWLEDGEMENTS

This research was supported by the Air Force Office of Scientific Research under Contract No. F49620-88-K-0006 and by NSF under Grant PHY87-06332.

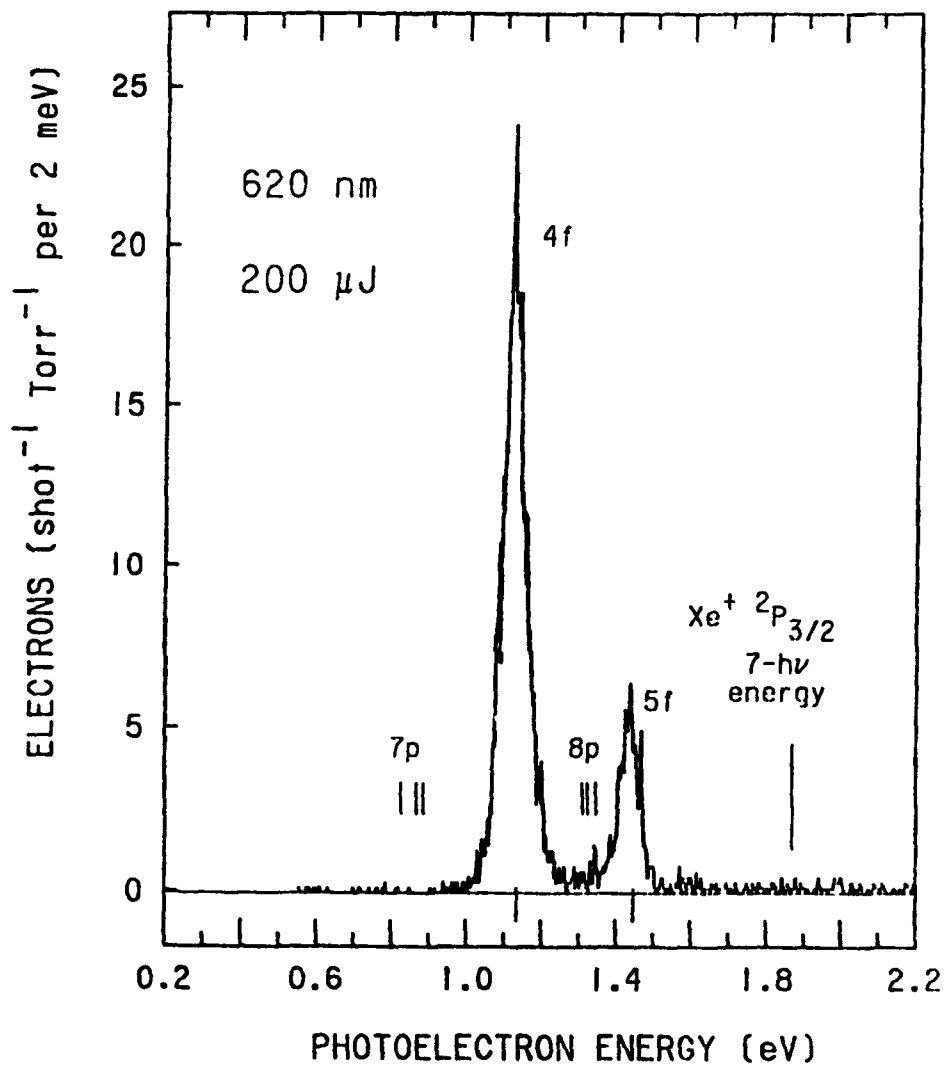
REFERENCES

1. R. R. Freeman, P. H. Bucksbaum, H. Milchberg, S. Darack, D. Schumacher, and M. E. Geusic, *Phys. Rev. Lett.* **59**, 1092 (1987).
2. T. J. McIlrath, R. R. Freeman, W. E. Cooke, L. D. van Woerkom, and T. J. McIlrath, *Phys. Rev. A* **40**, 2770 (1989).
3. P. Agostini, P. Breger, A. L'Huillier, H. G. Muller, G. Petite, A. Antonetti and A. Migus. *Phys. Rev. Lett.* **63**, 2208 (1989).
4. H. Rottke, B. Wolff, M. Brickwedde, D. Feldmann, and K. G. Welge, *Phys. Rev. Lett.* **64**, 404 (1990).
5. R. M. Potvelidge, R. Shakeshaft, *Phys. Rev. A* **41**, 558 (1990)
6. R. M. Potvelidge, R. Shakeshaft, *Phys. Rev. A* **41**, 1609 (1990)
7. M. D. Perry, A. Szoke and K. C. Kulander, *Phys. Rev. Lett.* **63**, 1058 (1989).
8. P. H. Bucksbaum, M. Bashkansky, and T. J. McIlrath, *Phys. Rev. Lett.* **58**, 349 (1987).
9. T. Tsuboi, E. Y. Xu, Y. K. Bae, and K. T. Gillen, *Rev. Sci. Instrum.* **59**, 1357 (1988).
10. E. Y. Xu, A. P. Hickman, R. Kachru, T. Tsuboi, and H. Helm, *Phys. Rev. A.* **40**, 7031 (1989).
11. D. S. Bethune, *Appl. Opt.* **20**, 1897 (1981).
12. M. J. Dyer, and H. Helm, submitted for publication.

13. C. E. Moore, *Atomic Energy Levels, Vol III, Circular of The National Bureau of Standards*, 467 (1958).
14. P. Agostini, A. Antonetti, P. Breger, M. Crance, A. Migus, H. G. Muller, and G. Petite, *J. Phys. B: At. Mol. Opt. Phys.* **22**, 1971 (1989).
15. P. Lambropoulos, X. Tang, P. Agostini, G. Petite, and A. L'Huillier, *Phys. Rev. A* **38**, 6165 (1988).

FIGURE CAPTIONS

- Figure 1. Energy spectrum of photoelectrons produced in seven-photon ionization of Xenon at 620 nm. The pulse duration is ~ 2 ps and the peak intensity is $\sim 3 \cdot 10^{13}$ W/cm².
- Figure 2. Laser Energy dependence of photoelectrons from multiphoton ionization of xenon at 620 nm. At a pulse width of ~ 2 ps the peak intensities are $\sim 3 \times 10^{13}$ W/cm² (bottom spectrum), $\sim 6 \times 10^{13}$ W/cm² (center spectrum), and $\sim 1.4 \times 10^{14}$ W/cm² (top spectrum). The energetic positions for the unshifted energy from 7, 8, and 9 photon ionization are indicated as well as the center positions of the 7p, 4f, and 5f manifolds as they would appear if their ac-Stark shift was purely ponderomotive.
- Figure 3. Same as Figure 2 but for a wavelength of 650 nm. The peak intensities are: $\sim 1.2 \cdot 10^{13}$ W/cm² (bottom), $\sim 2.2 \cdot 10^{13}$ W/cm² (center) and $\sim 4.4 \cdot 10^{13}$ W/cm² (top spectrum).
- Figure 4. Position of six-photon resonances in xenon as a function of laser intensity for two wavelengths, 620 and 650 nm. Four sets of data are shown: 1) The thin horizontal lines mark the position of even-parity states of xenon in the case that their ac-Stark shift is ponderomotive. 2) the two descending full lines give the energy of the six-photon dressed ground state (for 620 and 650 nm light) under the assumption that the ac-Stark shift of ground state xenon is negligible. 3) The full squares mark the absolute energies of resonance levels, obtained by subtracting the one-, two-, and three-photon energy from the sum of the ionization potential and the energy of the photoelectron peaks observed in seven-, eight-, and nine-photon ionization respectively. 4) The two open circles represent the position for the 6-photon resonant $7p[\frac{1}{2}]J = 0$ level, obtained in a second-order ac Stark calculation.²



sevup.kvs

Figure 1

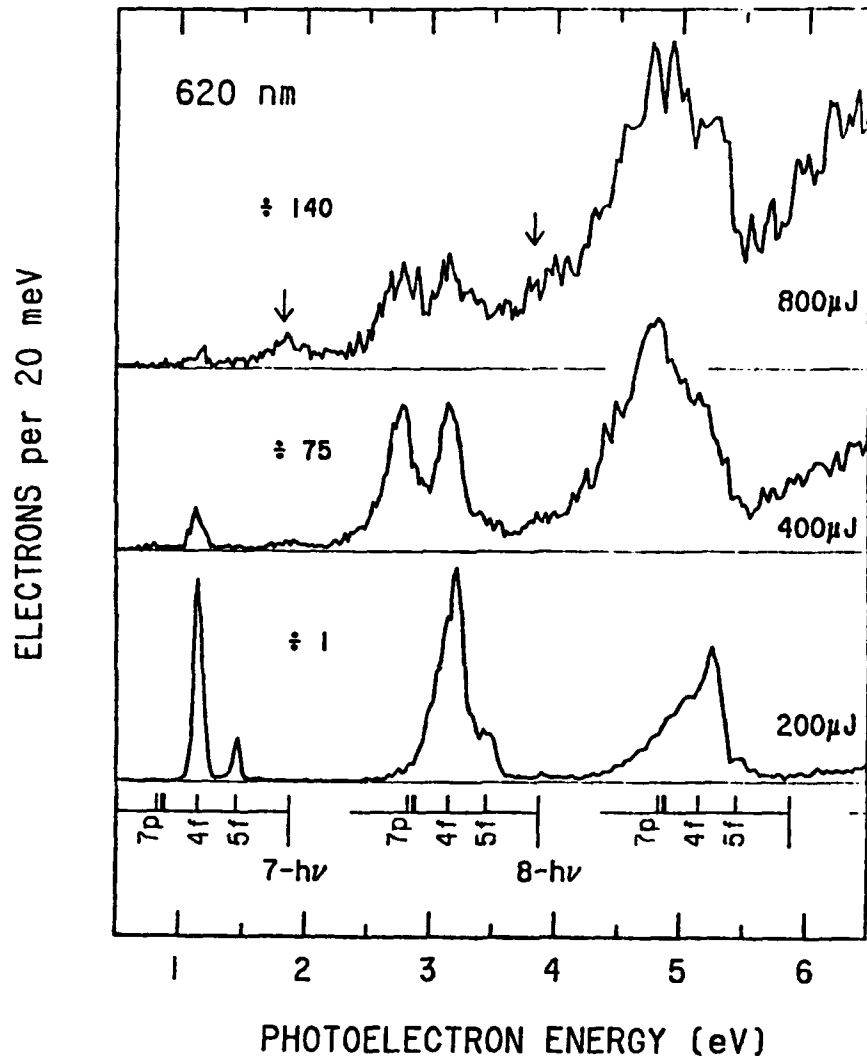


Figure 2

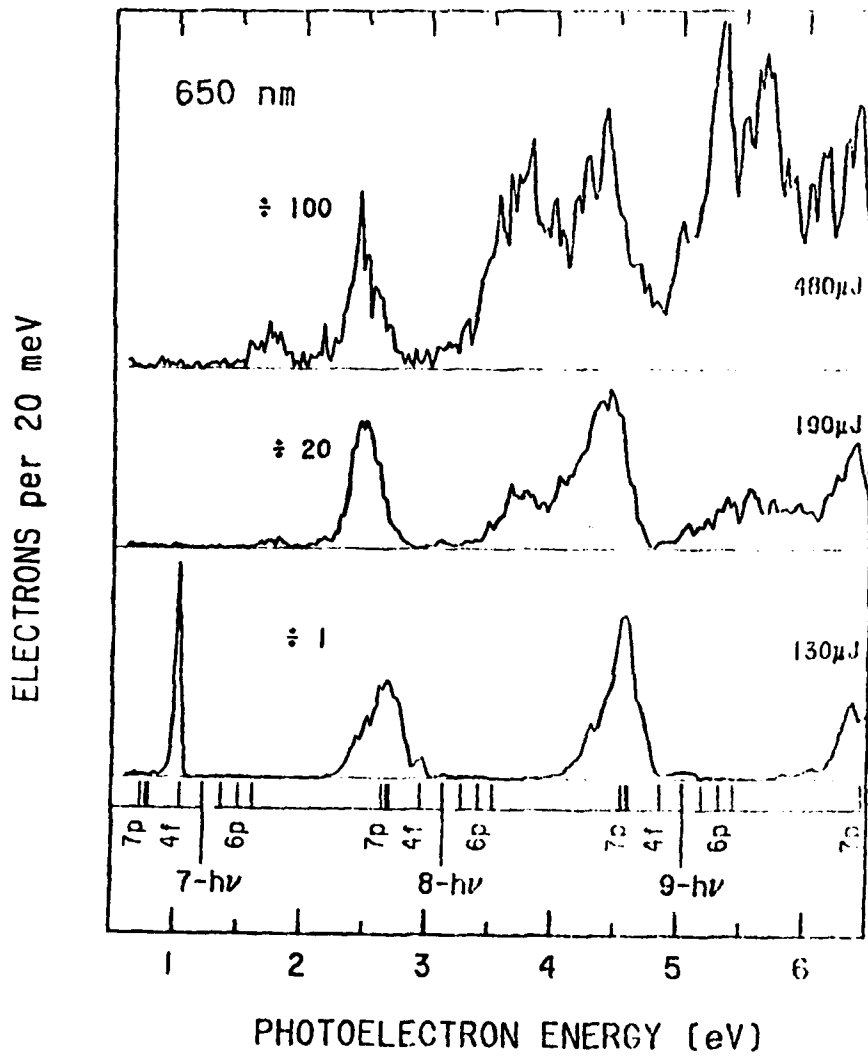


Figure 3

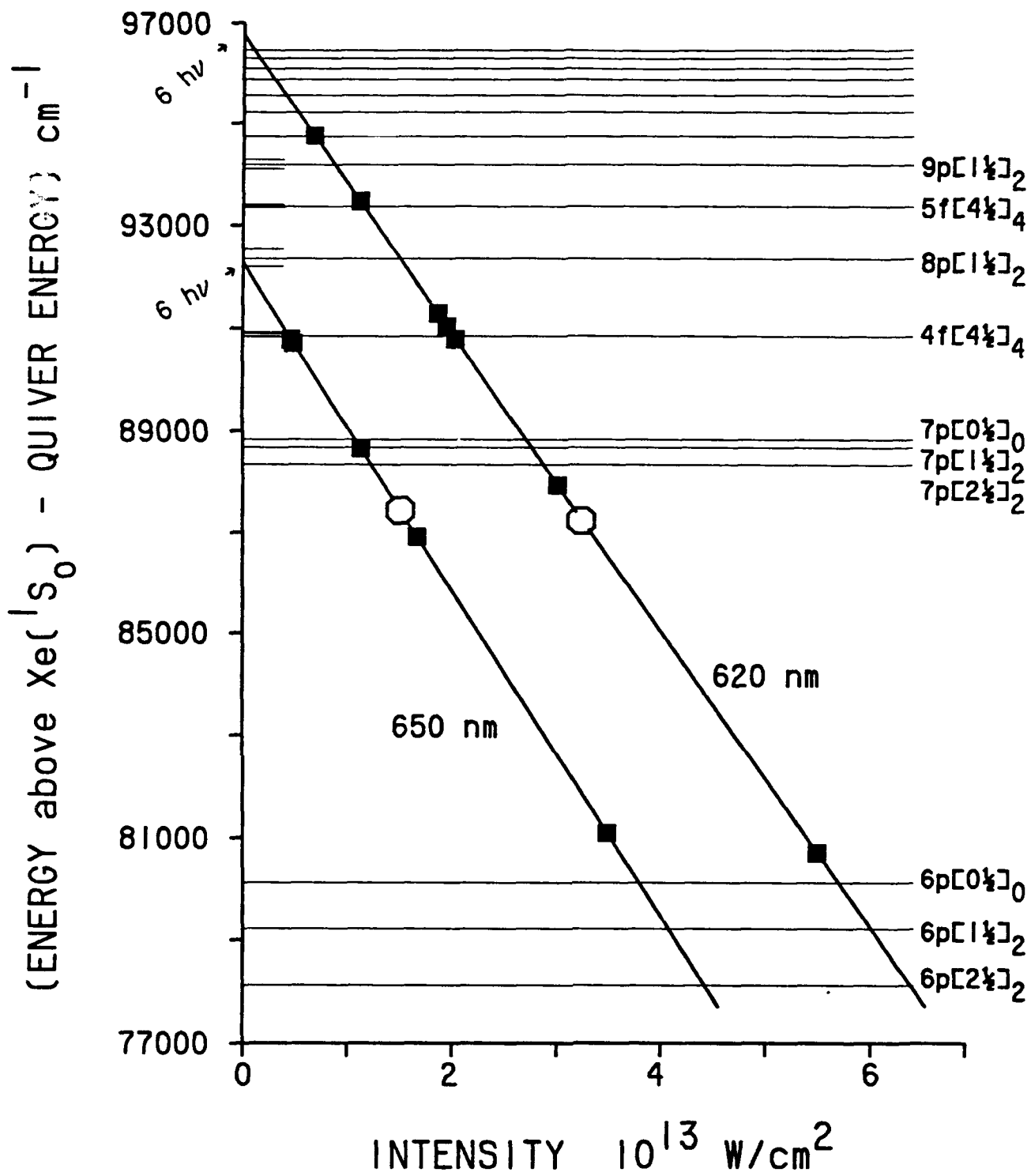


Figure 4

Appendix C

**PHOTODISSOCIATION DURING PHOTOIONIZATION IN
INTENSE LASER FIELDS**

PHOTODISSOCIATION DURING PHOTOIONIZATION IN INTENSE LASER FIELDS

H. HELM, M. J. DYER, H. BISSANTZ, D. L. HUESTIS

*Molecular Physics Laboratory
SRI International
333 Ravenswood Avenue
Menlo Park, CA 94025*

ABSTRACT

A high resolution photoelectron study of the response of molecular hydrogen to very intense laser fields ($>10^{13}$ W/cm²) at wavelengths between 309 and 330 nm shows that with increasing intensity direct multiphoton ionization of the molecule is surpassed by photodissociation of the neutral. This process leads to the formation of excited atomic hydrogen photofragments which are subsequently photoionized. Photoelectrons from this process form the dominant signature in the electron spectra at high field strength. The photoelectron spectra remain strongly dependent on wavelength at even the highest intensities investigated (8×10^{13} W/cm²). By contrast, the total ionization rate does not change perceptibly in the wavelength range studied.

The molecular response is discussed in the framework of combined effects of AC-Stark shifting of molecular Rydberg states and predissociation of the molecular Rydberg states induced by the intense laser field.

Introduction

At intensities above 10 TW/cm² atoms exhibit above threshold ionization (ATI) phenomena, that is they absorb more photons than required for ionization.¹⁻³ The photoabsorption is generally followed by emission of photoelectrons, and the measurement of the photoelectron energy is a primary diagnostic tool for ATI. Molecules respond similarly as atoms do, however an additional degree of freedom appears in the form of their dissociation continua. Thus in multiphoton excitation the dissociation process can be a competitor to ionization, or cause the photodissociation of the molecular ion produced. Photodissociation of neutral H₂ has been observed in many stepwise photo-excitation experiments and has been interpreted as resulting from sequential excitation, first to singly excited states, followed by excitation of the core electron.^{4,5,6}

Here we report observations of intensity-dependent photodissociation of H₂ that competes with the direct ionization channel. This phenomenon is seen as a manifestation of (1) the deformation of molecular bonds that arises from bound-free absorption of the molecular ion core and (2) the AC-Stark shifting of molecular Rydberg states in the intense laser field.

Experimental

The experiment is carried out in a magnetic bottle photoelectron spectrometer using light from a tunable dye-laser system with frequency doubling. The tunable oscillator is a synchronously pumped dye laser operating with DCM dye. The 3-500 mW average output of the dye laser is fed into 7m of single mode fiber to chirp and a double pass grating stage to compress the pulses down to 400 fs leading to an average output of typically 50 mW on the compressed light. Ten pulses of this train are amplified per second by a four stage amplifier system consisting of three Bethune prism cells with increasing bore diameters of 1, 3, and 6 mm. The beam is then expanded to a diameter of 20 mm and it double passes an open axicon amplifier. The amplifiers are pumped by a 4-ns 450-mJ frequency-doubled YAG laser at 532 nm. The final output at the red wavelengths is between 2 and 4 mJ at pulse lengths between 400 fs and 2 ps. Frequency doubling in KDP leads to pulses up to 1 mJ in energy.

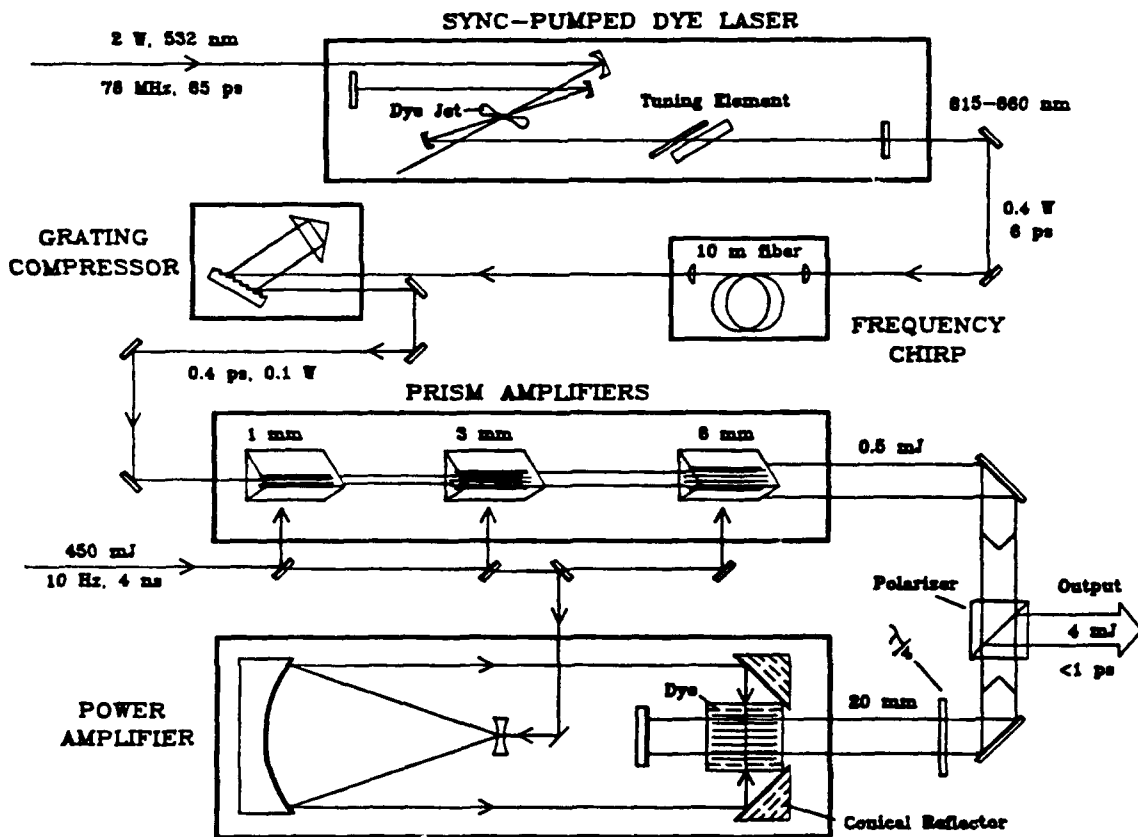


Figure 1. Schematic of dye laser system and amplifiers. The pulses from the synch pumped dye-laser are chirped and compressed and then amplified in three prism amplifiers. The final stage amplifier is a reflective axicon design for even amplification of the 20 mm diameter laser beam.

The photoelectron spectrometer is a magnetic bottle design⁷ that uses permanent magnets and a 64 cm time-of-flight section. The photoelectron signal is monitored by a constant fraction discriminator whose output feeds a chain of 16 time-to-digital converters, each with 1 ns resolution. The pressure in the interaction region is adjusted such that several (typically less than 10) electrons are recorded per laser shot. In studies of resonant ionization of H₂ at low intensity we have demonstrated⁸ a resolution of 50 meV at 1eV electron energy using this device. The laser energy is encoded with the arrival time of each electron detected and stored on hard disk of an IBM personal computer. Final data are restricted to laser energy bins that fall within $\pm 20\%$ of the quoted value. Experiments are carried out using linear laser polarization unless otherwise specified.

The base pressure in the photoionization region of the spectrometer is around 1×10^{-8} Torr, and the hydrogen pressure added reached as high as 5×10^{-6} Torr at the lowest intensities studied. The laser beam is focused using a 15 cm lens. Based on the near Gaussian and near diffraction limited beam profile we estimate the focal diameter ($1/e^2$) to be around 14 μm although a direct measurement of the focal properties at full power have not yet been carried out. All of the hydrogen work described below was obtained with the dye laser output of ~ 2 ps, obtained from autocorrelation measurements and assuming a sech² pulse shape. The bandwidth of the laser falls typically in the range of 5 \AA . Intensities quoted below are assumed lower limits, averaged over a conservatively chosen 20 μm spot diameter.

Experimental Results

The wavelength range chosen for this investigation is such that the three-photon energy lies below the C¹ Π_u state (3-photon threshold: 300 nm) while the four-photon energy lies near the ionization limit. Thus at the wavelengths employed here (309 -330 nm) three-photon resonances are only expected to involve the B¹ Σ_u^+ state while four-photon resonances may occur with a variety of vibrational levels of the Rydberg manifolds belonging to $n = 3$ and higher. We observed that scanning the dye laser in 5 \AA intervals over a portion of the wavelength range studied (328 to 318 nm) showed no noticeable wavelength dependence in the total ionization yield at intensities around 3×10^{13} W/cm². The yield was comparable at the other wavelengths investigated where photoelectron spectra were recorded at intervals of 25 \AA . Despite the insensitivity of the total ionization rate to wavelength we observe that the intensity distribution in the photoelectron energy spectra is strongly wavelength dependent.

In order to introduce the photoelectron features we first discuss relevant potential energy curves of molecular hydrogen. In Figure 2 we show a simplified diagram of molecular excited states, together with the lowest states of the molecular ion. Also indicated in this figure are the three, four, and five photon energies for photoexcitation at 325 nm, together with the vibrational wavefunction of ground state H₂, $v = 0$.

It is evident that in this case the Franck Condon overlap into the B¹ Σ_u^+ state is poor and that the first "good" resonant states occur at the four-photon energy. This leads us to assume that an important ionization channel may involve four-photon excited states of the molecule:



that are subsequently ionized by a fifth photon forming molecular hydrogen ions in specific vibrational levels v^+ :



Alternatively a non-resonant five photon process might occur



which could also form molecular hydrogen ions in a variety of vibrational levels.

The observation is that indeed, at low intensities, the spectra show photoelectrons with energies that are consistent with the formation of H_2^+ . As an example we give in Figure 3 spectra obtained at 3175 Å at various intensities.

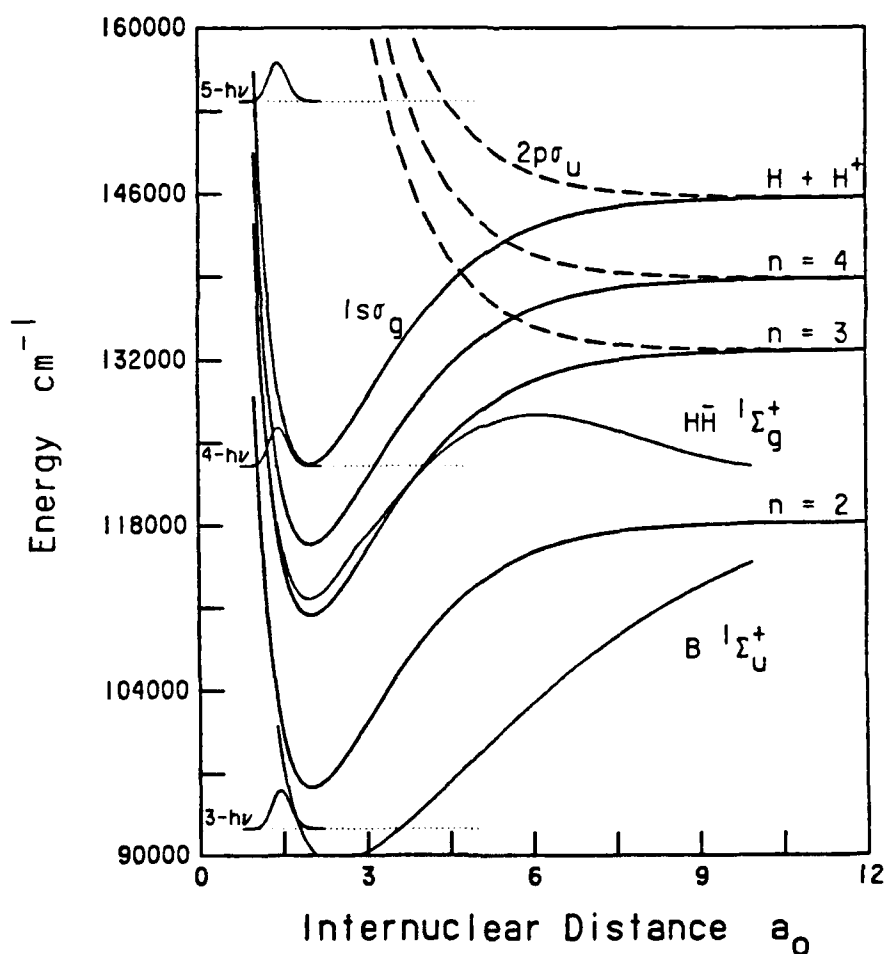


Figure 2. Selected potential energy curves of H_2 and the ground states of H_2^+ . Also indicated are the resonant energies for 3, 4, and 5 photons at 325 nm together with the vibrational wave function of $v = 0$ of ground state H_2 . The bound and repulsive Rydberg states are shown for zero quantum defect.

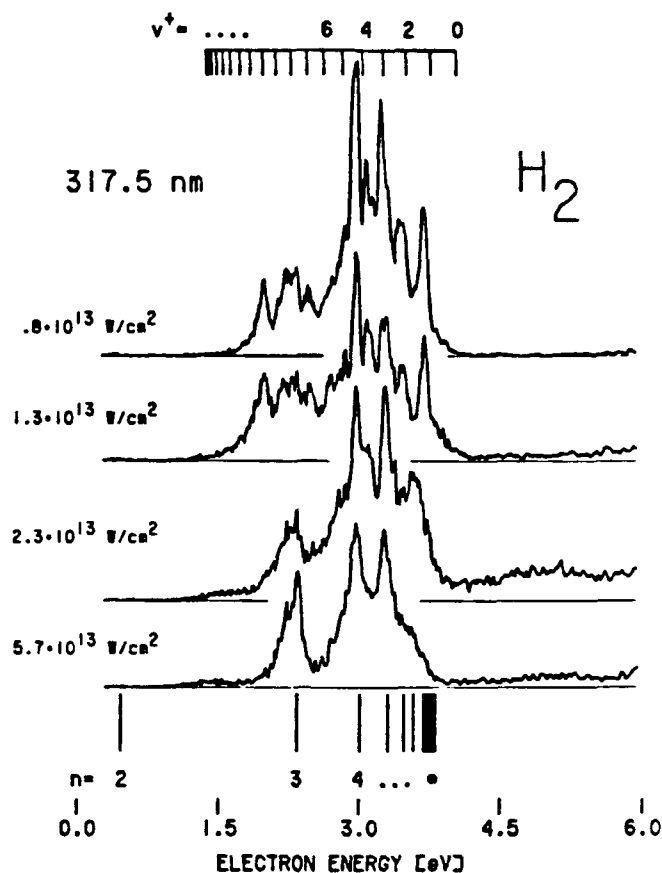
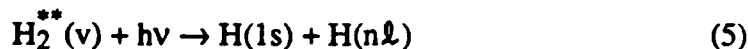


Figure 3. Photoelectron spectra of H₂ at 3175 Å as a function of intensity. The tickmarks at the top refer to photoelectron energies as they should appear from five-photon nonresonant ionization forming H₂⁺. The tickmarks at the bottom refer to photoelectrons produced in one-photon ionization of excited atomic hydrogen fragments H(nℓ).

The surprising observation in Figure 3 and in the spectra recorded at other wavelengths is that as the laser intensity is increased the photoelectron signal from the molecular hydrogen ion channel is apparently surpassed by the signal from one-photon ionization of excited atomic hydrogen



where $n \geq 3$. This observation is interpreted as being due to a multiphoton dissociation process. Plausible channels for the formation of excited atomic hydrogen are either the photodissociation of molecular Rydberg states:



or also dissociative ionization processes involving at least eight photons:



In Figure 3 we indicate at the top of the figure the electron energy peak location expected for non resonant five-photon ionization (process (3)) when the molecular ion is formed in the lowest rotational level. The one-photon ionization process of atomic hydrogen gives rise to a unique energy position that unambiguously identifies the excited atomic hydrogen fragment $H(n\ell)$ and the energies expected from process (4) are marked at the bottom of the figure. The rather distinct and simple features in the photoelectron spectrum at high intensities clearly suggest that reaction (4) is the dominant channel there.

As mentioned above we find that the intensity distribution in the photoelectron spectra is strongly wavelength dependent. This dependence exists at low intensities where the presence of many individual peaks indicates that processes (1-3) lead to the formation of H_2^+ ions in a variety of vibrational levels but also at higher intensities where the spectrum simplifies and specific atomic excited states are the dominant final products.

As an example we give in Figure 4 photoelectron spectra obtained at 3250 Å for a range of intensities. The spectra appear quite different from those obtained at 3175 Å. An additional surprising feature in the spectra in Fig. 4 is that the dissociation process tends to favor lower dissociation limits $H(n\ell)$ as the intensity grows. While dissociation into $H(n=3)$ is only a weak channel at the lowest intensity (see the lowest trace in Figure 4) this channel dominates the spectrum the highest intensity value. We also note in this figure the appearance of the first ATI peaks of the photoelectron spectra at the higher intensities. ATI peaks of similar magnitude are present at all other wavelengths studied.

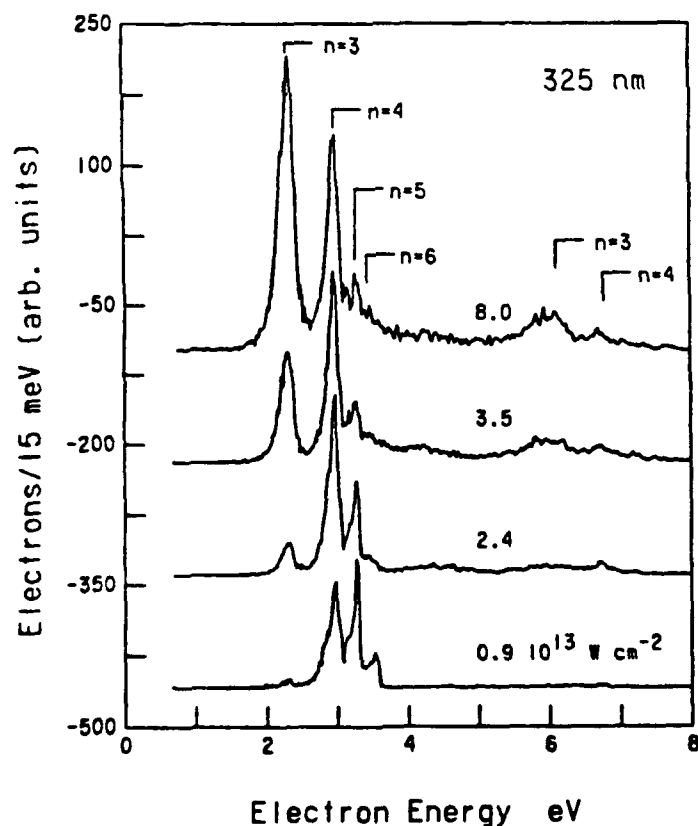


Figure 4. Photoelectron spectra of H_2 at 3250 Å as a function of intensity. An intensity dependent shifting of population into lower dissociation limits is apparent.

Discussion

Numerous papers have appeared in recent years on photoionization of molecular hydrogen in intense fields.⁹⁻¹² The sole common feature that can be extracted from reading this literature appears to be that the ionization process remains wavelength specific at even high intensities such that no single common rule has yet emerged. This fact is different from the atomic case where the dominant path appears when selected bound states are AC-Stark shifted into resonance - giving rise to specific ionization features that can be correlated with individual bound states.

The phenomenon of strong wavelength dependence is not surprising in view of the various electronic, vibrational and rotational degrees of freedom of the intermediate excited states that can participate in the multiphoton excitation process H_2 . The data presented here add another dimension to the ongoing discussion on molecular hydrogen in strong fields and their interpretation must be viewed as applicable to the specific wavelength range investigated. We have carried out similar studies at wavelengths from 610 to 660 nm and find photoelectron spectra that are quite different from those reported here in that individual peak structures are lost at high intensity at the red wavelengths.

Before we discuss the mechanism of photoionization and photodissociation via four-photon excited intermediate states to explain the observed photoelectron features we first discuss specific properties of the excited states of molecular hydrogen as well as the effect of ponderomotive forces on the appearance of the photoelectron spectra.

Potential Energy Diagram

The potential energy diagram for molecular hydrogen given in Figure 2 is highly schematic in its representation of the bound and dissociative Rydberg states. The states shown are drawn assuming zero quantum defect. The full diagram known to date for the excited singlet manifold of states is considerably more dense owing to the fine structure arising from the non zero quantum defects of the various ℓ -components in each principal quantum number. Furthermore, the avoided crossings¹³ between states of the same symmetry that are either the singly excited Rydbergs (orbital configuration $(1s\sigma_g)(n\ell\lambda)$) or the doubly excited states $(2p\sigma_u)(n\ell\lambda)$ modify the appearance of the adiabatic states at large ($R > 4a_0$) internuclear distances. In addition, the $^1\Sigma$ state potential energy curves are modified at large separation by the strongly attractive ion-pair character. This is apparent for the $B^1\Sigma_u^+$ and the $H^1\Sigma_g^+$ curves which are included in Figure 2.

Despite these simplifications the potential energy diagram in Figure 2 serves to indicate the strongest transition expected for reaching excited states at the wavelengths considered in this paper: At the internuclear distance of the vibrational wavefunction of the $v = 0$ level of the ground state of H_2 , a vertical multiphoton excitation may find a first energy resonance with either the $B^1\Sigma_u^+$ state (3-photon transition) or else with the gerade states of the manifolds $n = 3$ or higher at the four photon energy. At the short internuclear separation where vertical excitation can be efficient the latter are nearly purely the singly excited states $(1s\sigma_g)(n\ell\lambda_g)$ with $\ell = s, d, f$ and h . At the wavelengths of this experiment the Franck-Condon factors to reach the bound B-state levels is always at least an order of magnitude smaller than the best overlaps with vibrational levels of the four-photon excited states. We therefore initially concentrate on ionization processes that involve four photon

excitation of H_2 to the bound Rydberg states and only later discuss the role of three-photon resonances with the B-state.

Ponderomotive Effects

When photoelectron energy spectra are recorded with intense lasers and short pulse lengths it is paramount to consider the effect that the ponderomotive forces can have on the measured photoelectron energy. We note that the pulse lengths utilized here (~ 2 ps) are sufficiently small, and the interaction volume sufficiently large ($\geq 15 \mu\text{m}$) such that the ponderomotive energy is not recovered by slow photoelectrons because they cannot exit the laser focus during the time of the laser pulse. To prove this point we used our laser in a photoionization experiment in xenon for which numerous previous data exist for comparison. We show a typical photoionization spectrum of xenon recorded at 620 nm in Figure 5. At this wavelength seven photons are required to reach above the zero-field ionization threshold. We have marked in the figure where photoelectrons were expected

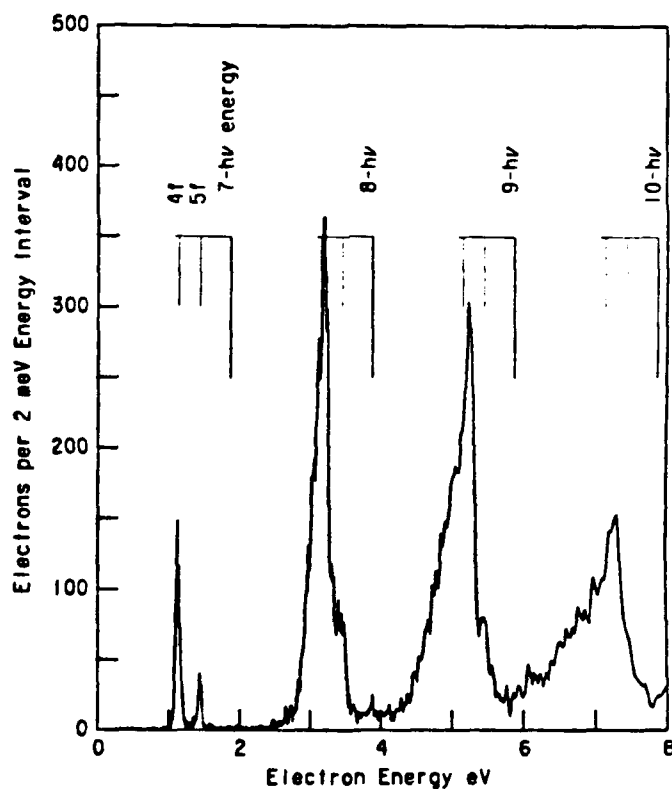


Figure 5. Photoelectron energy spectrum obtained in xenon at $\sim 3 \cdot 10^{13} \text{ W/cm}^2$. The pulse length is 2 ps and the wavelength is 6200 Å. The Photoelectron peak position expected from non-resonant 7-photon ionization to form $\text{Xe}^+(^2P_{3/2})$ is marked at the top of the figure. The peak energies in the 7-photon peaks as well as the higher ATI peaks are consistent with resonant excitation via the 4f and 5f resonance levels.

from non-resonant seven photon ionization to form $Xe^+(^2P_{3/2})$. We note that the observed electron energy peaks are shifted to lower energies by an amount that is consistent with the process¹⁻³ where a six-photon resonance of bound neutral xenon is shifted into resonance as the intensity of the field grows and is subsequently ionized by an additional photon. To the extent that the excited states that form intermediate resonances experience an AC-Stark shift that is similar to the ponderomotive shift of the free electron

$$\epsilon_p = 750 I \lambda^2 \text{ (cm}^{-1}\text{)} \quad (7)$$

the photoelectron's kinetic energy in the field is reduced from that of the non-resonant process

$$E_e = 7 h\nu - IP \quad (8)$$

by an amount equivalent to ϵ_p . In Eq. 7, I is the laser intensity in units of 10^{12} W/cm² and λ is the wavelength in μm . The ponderomotive energy of Eq. 7 is converted into kinetic energy of the electron if the laser is on over a time span sufficient for the electron to "surf" off the focal volume¹⁵ thereby converting the gradient of the ponderomotive potential into kinetic energy. If on the other hand the laser pulse is short compared to the time required to exit from the focal region the ponderomotive energy remains with the electromagnetic field and the electron's energy is given by

$$E_e = 7 h\nu - IP - \epsilon_p \quad (9)$$

For an orientation to the magnitudes involved we note that an electron of 2.7 eV energy travels 1 μm in 1 ps. The energy positions in the photoelectron spectra in Figure 5 indicate that the intermediate states 4f and 5f are the dominant contributors to the ionization process in xenon at this wavelength and that the AC-Stark shift of these states is quite similar to that given by Eq. 7 for the free electron. We note that no contributions from intermediates of the 7p and 8p manifolds of xenon appear and that this shifted resonance structure is reproduced in the higher order ATI peaks although the experimental resolution diminishes somewhat there.

Therefore we expect that under the laser pulse and focal properties employed in our experiment on molecular hydrogen the ponderomotive shifts of the free electron are not recovered from the electromagnetic field.

Wavelength Dependence

The absence of any marked wavelength dependence in the total photoionization yield indicates that either a non-resonant ionization process dominates over one that utilizes resonant intermediates or else that the manifold of excited states that participate in resonant intermediate formation is sufficiently dense as well as sufficiently broadened by the presence of the intense laser field such that excited state ro-vibrational resonance structures merge into a quasi-continuum. At least three processes can be identified that contribute to this broadening, and most likely all three participate with varying degree in our experiment.

For one, an energy broadening of the excited state will arise from the short lifetime of the excited state against one-photon ionization. Typical values for these lifetimes can be calculated using the generalized cross section formula given by Huestis.¹⁶ A value of

200 fs is obtained for $n = 4$ at 10^{13} W/cm². It is quite evident that one-photon ionization of excited states should be quite efficient.

A second process responsible for broadening is related to the intensity dependent lifetimes of the molecular Rydberg states against photodissociation. We note here that this process involves the core electron of the Rydberg and we will discuss this process in detail in the next section.

A third factor is that even if no resonance appears at the four-photon energy at zero field, the AC-Stark shift of the excited states can shift rovibrational excited states into resonance at sufficient intensity, giving the appearance of continuous, wavelength-independent ionization. While the exact magnitude of the AC Stark shifts are not known, an order of magnitude estimate may be obtained from the ponderomotive shift (Eq. 7). At our wavelengths ϵ_p is about 100 mV per 10^{13} W/cm². The process of shifting intermediates into resonance is known to dominate atomic photoionization¹⁻³ at high fields and the example of xenon given in Figure 5 falls under this category. It is tempting to suspect a similar process in the molecular case but we must also consider the possibility of purely non resonant ionization.

If non-resonant ionization were an important contribution at our wavelengths then we would expect that the wavelength dependence of the electron energies formed in process (1) follows a five-photon dependence. This is contrary to what we find in the electrons' spectra. We show in Figure 6 the location of the dominant electron energies observed at the various wavelengths. It appears from the guiding lines drawn at a slope of one that

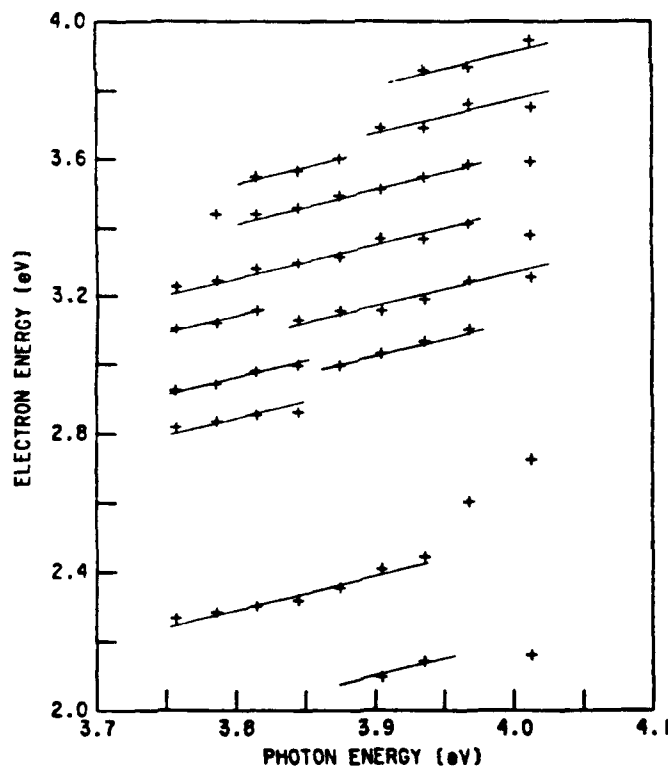


Figure 6. Energy of dominant features of the photoelectron spectra at wavelengths between 309 and 330 nm. Most peak positions follow short segments of slope of one, indicating that one-photon ionization of bound states that are AC-Stark shifted into resonance is the origin of these photoelectrons.

most peaks fall onto segments that vary with the one-photon energy. Also - if the five-photon process occurs in a purely non-resonant fashion at the intensities utilized in this work we would expect that the variation in the ponderomotive shift of the photoelectrons that are created at widely different intensities should lead to a distribution of electron energies for each final state v^+ generated.

We conclude that the most likely ionization channels involve four-photon excited intermediates that are shifted into resonance at a specific intensity. The photoionization of the shifted state will lead to a photoelectron energy that shifts linear with the one-photon energy over a wavelength range over which the Stark shift can be accomplished by the intensities employed.

Four-Photon Resonance Formation

The existence of four-photon resonant intermediates can be used to develop a picture that can explain the observed shifting from ionization of excited H_2 to dissociation into neutral fragments and it can also convey the origin for the switching to lower dissociation limits $H(n\ell)$ as the intensity grows.

One aspect of this picture involves the AC Stark shift of the Rydberg electron. At 50 TW/cm^2 the ponderomotive energy of a free electron amounts to 0.5 eV. If the highly excited states of H_2 experience AC-Stark shifts like that of a free electron, then the excited state manifold will shift upwards with respect to the four-photon dressed ground state as the intensity grows.

It would thus appear that bound states that lie for zero field strength at energies below the four-photon energy can be shifted into resonance as the intensity grows. Ionization may then be envisioned to occur whenever the four-photon dressed ground state encounters a resonance with good transition strength. This picture similar to that generally accepted in the atomic ionization case.

The open question is of course what is the actual Stark shift of the four-photon excited states at high field strength. At the wavelengths used here no bound transitions can be driven with one photon from Rydberg states with $n \geq 3$. A good first-order assumption may therefore be that the AC-stark shift of the higher Rydberg states is comparable to that of the free electron. However how will the core respond to the field? In the classical picture of a Rydberg state we may consider the ionic core as being separate from the Rydberg orbital. If we neglect electrostatic shielding of the core by the Rydberg orbital we should consider the response of the isolated core ion, H_2^+ to the field. This response has been the subject of several recent papers and we use the picture developed by Bandrauck et al.¹⁷ and Gusti et al.¹⁸ in the following discussion.

Dressed State Picture

We now combine the predicted response of the isolate core ion¹⁸ with the picture of a Rydberg electron that experiences an AC-Stark shift as if it were a free electron. This leads to a potential energy diagram of adiabatic potential energy curves such as shown in Figure 7. The full curves give a simplified representation of the Rydberg states that originate from the dissociation limits $H(1s) + H(n = 3)$ and $H(1s) + H(n = 4)$, calculated for a field strength of 50 TW/cm^2 . The unperturbed ground state of H_2^+ is indicated by the dashed line and the 4-photon energy at 325 nm is indicated at the left. The potential energy

curves are the results of a Floquet calculation¹⁸ that we performed for the diabatic singly and doubly excited states, $1s\sigma_g n\lambda_g$ and $2p\sigma_u n\lambda_u$, for 50 TW/cm^2 . In this calculation the Rydberg states with $n = 3$ and $n = 4$ are considered separately, with no matrix element connecting them. In the dressed state picture the coupling between the singly excited gerade states and the doubly excited ungerade states leads to avoided crossings between the states $\{(n = 3)\text{gerade} + \text{even photon number}\}$ and $\{(n = e)\text{ungerade} + \text{odd photon number}\}$, with different numbers of photons, N , and likewise for $4g$ and $4u$. At molecular distances this coupling reduces the number of bound states, and remaining bound states are affected by predissociation through higher order couplings with the continua labelled $3,4g \text{ } N = 2$ and $3,4u \text{ } N = 3$.

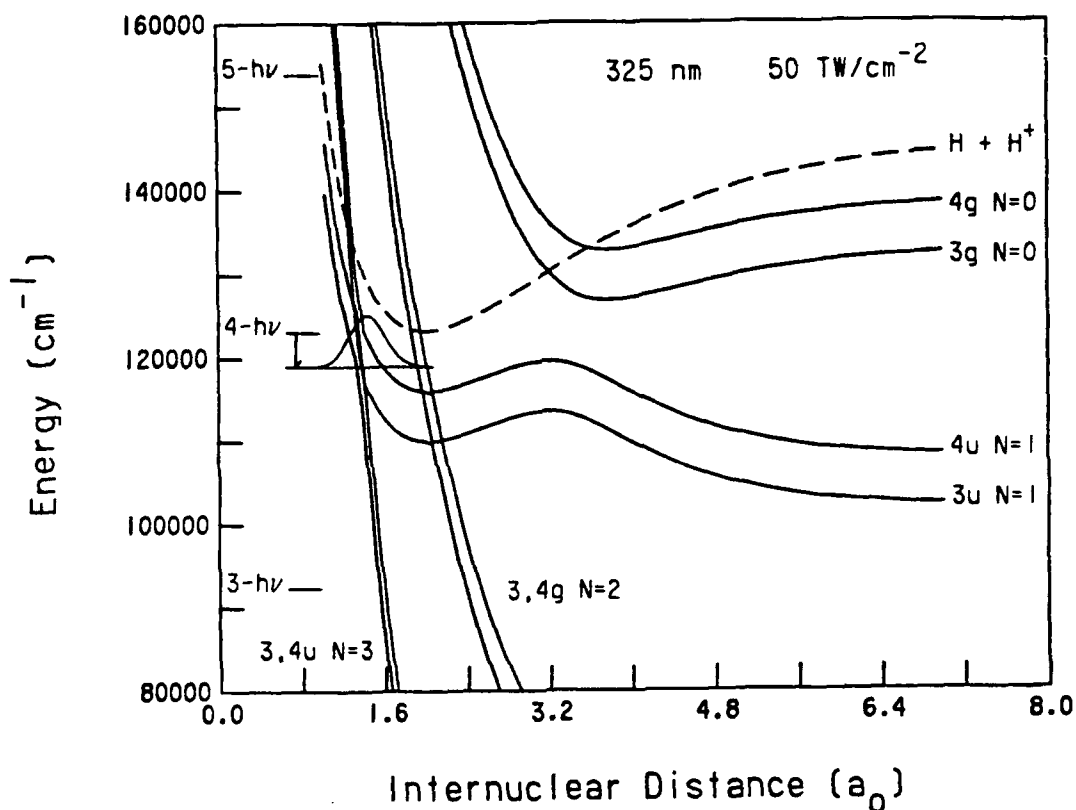


Figure 7. Results of a Floquet calculation for the $n=3$ and $n=4$ states of H_2 with the orbital configurations $1s\sigma_g n\lambda_g$ and $2p\sigma_u n\lambda_u$ at 50 TW/cm^2 and 325 nm . The ponderomotive shift for the location of the four photon energy relative to the unperturbed potential energy curve of H_2^+ (dashed curve) is also indicated.

As the intensity of the laser field increases a reduction of the number of bound levels occurs in the excited state manifolds and concurrent with this effect the four-photon resonant energy continually sweeps through the excited state manifold. In this fashion an intensity dependent competition between neutral dissociation and ionization occurs because with increasing intensity the higher vibrational levels in the Rydberg states will appear as continuum states that dissociate rapidly. The classical times for dissociation of molecular hydrogen is extremely short, it takes typically 10 to 20 fs to accelerate to distances of 10 \AA . Consequently dissociation in competition with direct ionization of the neutral excited

molecule is rather plausible in this adiabatic picture. Concurrent with opening the molecular bonds of the Rydberg the shifting of states in energy at short internuclear distance leads to a progressively better overlap with states from lower principal quantum number - thereby explaining the switching to lower dissociation limits as the intensity increases.

Conclusions

The wavelength and intensity dependence of photoelectron energies observed from molecular hydrogen at intensities above 10^{13} W/cm² and at wavelengths where five photons are required to reach the ionization continuum show that the most likely ionization channels involve four-photon excited intermediate states from the Rydberg manifolds with $n = 3 - 6$. While specific rovibrational assignment of these states cannot be given at this point (primarily because little experimental information exists about hydrogen states at these high energies) this identification allows to develop a framework of the behavior of molecular Rydberg states in intense fields. This framework should be generally applicable to molecules in strong fields.

In molecular Rydberg states the AC-Stark effects on both the Rydberg electron and on the core ion need to be taken into account. If the core ion has a transition that is strongly driven by the applied electromagnetic field then the core's response to the field must play a major role. In the framework of dressed states that are adiabatic in the electromagnetic interaction the core's response results in both a level shift (that is generally opposite to the direction of the ponderomotive shift of a free electron) and in a level broadening owing to predissociation and dissociation. The combination of this effect with the AC-Stark shifting of the Rydberg orbital provides a qualitative explanation of the observed switching from ionization to form H_2^+ to dissociation into neutral excited atomic hydrogen, as well as the observed switching in dissociation to progressively lower dissociation limits as the intensity grows.

This simple discussion of a Rydberg electron and a core ion that respond independently of each other to the electromagnetic field appears useful in rationalizing the experiments performed. There remain many quantitative questions that need to be investigated both experimentally and theoretically.

Acknowledgments

This research was supported by the National Science Foundation under grant number PHY-87-06332 and by the Air Force Office of Scientific Research under Contract No F49620-88-K-0006.

References

1. R. R. Freeman, P. H. Bucksbaum, H. Milchberg, S. Darack, D. Schumacher, and M. E. Geusic, *Phys. Rev. Lett.* **59**, (1987) 1092.
2. T. J. McIlrath, R. R. Freeman, W. E. Cooke, L. D. van Woerkom, and T. J. McIlrath, *Phys. Rev. A* **40**, (1989) 2770.
3. P. Agostini, P. Breger, A. L'Huillier, H. G. Muller, G. Petite, A. Antonetti, and A. Migus, *Phys. Rev. Lett.* **63**, (1989) 2208.

4. J.H.M. Bonnie, J.W.J. Verschur, H. J. Hopman, and H. B. van den Linden van den Heuvell, *Chem. Phys. Lett.* **130**, (1986) 43.
5. M. A. O'Halloran, S. T. Pratt, P. M. Dehmer, and J. L. Dehmer, *J. Chem. Phys.* **87**, (1987) 3288.
6. E. Y. Xu, T. Tsuboi, R. Kachru, and H. Helm, *Phys. Rev. A* **36**, (1987) 5645 .
7. T. Tsuboi, E. Y. Xu, Y. K. Bae, and K. T. Gillen, *Rev. Sci. Instrum.* **59**, (1988) 1357.
8. E. Y. Xu, A. P. Hickman, R. Kachru, T. Tsuboi, and H. Helm, *Phys. Rev. A* **40**, (1989) 7031.
9. T. S. Luk and C. K. Rhodes, *Phys. Rev. A* **38**, (1988) 6180.
10. J.W.J. Verschuur, L. D. Noordam, and H. B. van Linden van den Heuvell, *Phys. Rev. A* **40**, (1989) 4383.
11. A. Zariyev, P. H. Bucksbaum, H. G. Muller, and D. W. Schumacher, *Phys. Rev. A* **42**, (1990) 5500.
12. S. Allendorf, in press (1991).
13. L. J. Lembo, N. Bjerre, D. L. Huestis, and H. Helm, *J. Chem. Phys.* **92**, (1990) 2219.
14. P. Avan, C. Cohen-Tannoudji, J. Dupont-Roc, and C. Fabre, *Le Journal de Physique* **37**, (1976) 993.
15. P. H. Bucksbaum, M. Bashkansky, and T. J. McIlrath, *Phys. Rev. Lett.* **58**, (1987) 349.
16. D. C. Lorents, D. J. Eckstrom, and D. Huestis, "Excimer formation and decay processes in rare gases," Report No. MP 73-2, Stanford Research Institute, Menlo Park, CA (September 1973).
17. A. D. Bandrauk and N. Gélinas, *J. Chem. Phys.* **86**, (1987) 5257.
18. A. Guisti-Suzor, X. He, O. Atabek, and F. H. Mies, *Phys. Rev. Lett.* **64**, (1990) 515.